scientific reports

Check for updates

OPEN

Eco-friendly biosynthesis of gold nanoparticles from *Amphimedon compressa* with antibacterial, antioxidant, anti-inflammatory, anti-biofilm, and insecticidal properties against diseases vectors

Alsayed E. Mekky[1], Ebrahim Saied[1], Mahmoud M. Al-Habibi[2], Zeinab A. Shouaib[3], Ahmed I. Hasaballah[4], Mohammed E. Rashed[5], Ashjan F. Khalel[6], Amal Naif Alshammari[6], Fady Sayed Youssef[7], Ahmed M. Al-Shahat[4], Mohammad Y. Alfaifi[8,9], Serag Eldin I. Elbehairi[8,9], Mohammed Aufy[10,11]✉ & Tharwat A. Selim[4]✉

Gold nanoparticles (AuNPs) are increasingly recognized for their potential in biology due to their excellent drug delivery capabilities and ease of synthesis. To create AuNPs using marine sponge *Amphimedon compressa*, we used several techniques, including ultraviolet–visible (UV–visible) spectrophotometry, Fourier transform infrared (FTIR) spectrophotometry, scanning electron microscopy (SEM), transmission electron microscopy (TEM), and x-ray diffraction (XRD). The UV–visible spectroscopy results demonstrated the formation of stable AuNPs at a pH of 7, with a peak absorption at 564 nm. FTIR spectroscopy indicated that secondary metabolites featuring –OH functional groups acted as reducing agents in the production of AuNPs. Morphological analysis showed that the AuNPs were spherical, consistently shaped particles averaging 10–40 nm in diameter, with proven stability over time. The inhibition zones for the bacteria tested with the synthesized AuNPs varied from 26 to 31 mm. Both the AuNPs and the *A. compressa* extract displayed significant antioxidant activity, achieving DPPH radical scavenging percentages of 70.73% and 85.62%, respectively. In terms of anti-inflammatory activity, the AuNPs showed dose-dependent anti-inflammatory activity, with hemolytic inhibition percentages of 4.8%, 10.2%, 12.8%, 14.9%, 19.5%, and 22.4% at increasing concentrations. Furthermore, both the crude extract and the synthesized AuNPs exhibited adulticidal activity against the house fly (*Musca domestica*) and the mosquito (*Culex pipiens*). The LC_{50} and LC_{90} values for the crude extract were 34.988 and 62.836 ppm for *M. domestica*, and 9.258 and 17.399 ppm for *C. pipiens*. For the AuNPs, the corresponding values were 8.545 and 15.157 ppm for *M. domestica*, and 7.573 and 14.074 ppm for *C. pipiens*. Adult mortality caused by the AuNPs extract reached 100.00% for both *Musca domestica* and *Culex pipiens* at a concentration of 6 ppm. Overall, *M. domestica* and *C. pipiens* were more sensitive to AuNPs than to the crude extract. Both the synthesized AuNPs and the crude extract caused a significant, dose-dependent reduction in fecundity and hatchability in *M. domestica* and *C. pipiens*. In conclusion, the marine sponge *A. compressa* serves as an effective biological source for the synthesis of AuNPs, which demonstrate significant antibacterial, antioxidant, anti-inflammatory, anti-biofilm, and insecticidal activities, highlighting their potential in biomedical and environmental fields.

Keywords Nanotechnology, AuNPs, Antibacterial, Marine sponge, Biosynthesis, anti-inflammatory, anti-biofilm, Adulticidal activity, insecticidal properties

[1]Botany and Microbiology Department, Faculty of Science (Boys), Al–Azhar University, Nasr, Cairo 11884, Egypt. [2]Microbiology and Immunology Department, Faculty of Pharmacy (Boys), Al-Azhar University, Cairo, Egypt. [3]Zoology and Entomology Department, Faculty of Science, (Girls), Al-Azhar University, Nasr, Cairo 11884, Egypt. [4]Zoology

and Entomology Department, Faculty of Science (Boys), Al-Azhar University, Nasr, Cairo 11884, Egypt. [5]Research Institute of Medical Entomology, Ministry of Health and Population, Dokki, Giza, Egypt. [6]Biology Department, Al-Darb University College, Jazan University, Jazan, Saudi Arabia. [7]Pharmacology Department, Faculty of Veterinary Medicine, Cairo University, Giza 12211, Egypt. [8]Faculty of Science, Biology Department, King Khalid University, 9004 Abha, Saudi Arabia. [9]Tissue Culture and Cancer Biology Research Laboratory, King Khalid University, 9004 Abha, Saudi Arabia. [10]Departmet of Pharmaceutical Sciences, Division of Pharmacology and Toxicology, University of Vienna, Vienna, Austria. [11]Departmet of Pharmaceutical Sciences, Division of Pharmaceutical Chemistry, University of Vienna, Vienna, Austria. ✉email: mohammed.aufy@univie.ac.at; tharwat3d@azhar.edu.eg

Nanoparticles are utilized in numerous fields, including biomedicine, nutraceuticals, medicinal chemistry, drug delivery systems, materials science, and environmental pollution management[1]. Traditional methods for synthesizing and stabilizing metal nanoparticles have included chemical and mechanical processes, electrochemical techniques, photochemical reactions in reverse micelles, and, more recently, methods rooted in green chemistry[2]. Despite the development of various physical and chemical techniques for creating metal nanoparticles, these approaches often come with high costs and require the use of hazardous and harsh chemicals for reduction and stabilization purposes. The eco-friendly synthesis of nanoparticles comprises choosing solvents that are safe for the environment, along with reducing and stabilizing agents that do not harm the ecosystem[3,4]. Various natural sources, including microbes, sea algae, plant tissues, extracts, fruits, and other plant-derived substances, are employed in the production of nanomaterials, highlighting the shift towards more sustainable practices in nanoparticle synthesis[5]. In the biomedical and pharmaceutical sectors, the concept of green chemistry is guiding the synthesis of various metallic nanoparticles. Gold is a favored material for nanotechnology applications because of its unique physicochemical properties, which include its chemical inertness and resistance to surface oxidation. Gold nanoparticles (AuNPs) have undergone extensive research and are becoming vital for drug delivery systems, attributed to their stability, adaptable surface characteristics, and low cytotoxicity under in vivo conditions[6]. The global health sector is currently facing a significant challenge as many antibiotics have become ineffectual in treating or preventing microbially induced infectious illnesses. Historically, antimicrobial agents were key in managing infections from bacteria or fungi[7]. However, the emergence of dangerous, antibiotic-resistant bacteria poses a substantial threat. Microorganisms are developing resistance to antimicrobial drugs through methods such as enzymatic deactivation, modification of drug target sites, reduced cell wall permeability to antibiotics, and efflux mechanisms[8,9].

The World Health Organization (WHO) reports that microbial diseases are responsible for approximately 0.7 million deaths annually[10]. Without the development of effective drugs to manage or eliminate these pathogenic microorganisms, deaths attributable to microbial diseases are projected to increase to around 10 million by the year 2050[11]. Identifying compounds that can inhibit the growth of these pathogens, particularly those resistant to current medications, remains a key priority. AuNPs have been recognized as promising antimicrobial agents capable of hindering microbial growth and addressing the growing issue of antimicrobial resistance to conventional antibiotics[12]. They are widely used for their anti-inflammatory, antibacterial, and antifungal properties in various applications, including wound dressings, dental care, eye treatments, sterilization of medical equipment, and coatings for catheters[13].

Previously, it was believed that bacteria predominantly existed in a free-floating, or planktonic, state. However, it has since been discovered that most bacteria form complex structures known as biofilms[14]. These biofilms are intricate systems consisting of bacterial communities enveloped in extracellular polymeric substances (EPS), which serve as a protective barrier against the external environment. Biofilms exhibit a change in the expression of many phenotypes, particularly those related to virulence, when compared to bacteria in a planktonic state[15]. This is underscored by estimates from the National Institutes of Health (NIH), which suggest that approximately 80% of infections are initiated and sustained by biofilms[16]. Key foodborne pathogens include species such as *Acinetobacter* spp., *Bacillus cereus*, *B. subtilis, Campylobacter jejuni, Serratia marcescens, Escherichia coli, Klebsiella spp., Listeria monocytogenes, Staphylococcus aureus, and Vibrio cholerae*, among others[17,18]. Reactive oxygen species (ROS) produced during bacterial infection or inflammation often associated with biofilm formation can induce oxidative stress in host tissues. To counteract this, antioxidant molecules play a critical role as free radical scavengers[19]. These compounds neutralize and eliminate free radicals by donating hydrogen atoms, thereby protecting biological systems from oxidative damage[20].

Flies and mosquitoes are among the most common vectors of diseases affecting human health. The most frequent fly to infiltrate homes and the surrounding area is the house fly, *M. domestica L.,* whose presence is interpreted as an indicator of unsanitary environments. It is capable of transmitting various pathogens, including helminths and bacteria that cause gastrointestinal illnesses such as dysentery and diarrhea. In livestock environments, *Musca domestica* is also a significant pest, contributing to disease transmission and resulting in economic losses and animal discomfort[21]. Similarly, the mosquito *C. pipiens* is a major vector in urban and semi-urban areas of Asia and Africa, primarily responsible for the transmission of lymphatic filariasis[22]**.** This species has a broad global distribution and is associated with the spread of multiple diseases[23]. Effective control of flies and mosquitoes is essential for reducing the incidence of vector-borne diseases and improving overall public health and quality of life[24].. Although synthetic insecticides such as organochlorines and organophosphates are widely used for insect control, including (Malathion and Diazinon) for house flies, and (Temephos and Permethrin) for mosquito larvae, their efficacy is often limited due to resistance development, environmental toxicity, and economic constraints[25,26]. As a result, plant- and marine-derived products have gained attention as eco-friendly alternatives for vector control[27,28].

The marine sponge *Amphimedon compressa* belongs to family Niphatidae, order Haplosclerida and class Demospongiae. This sponge typically grows to a length of up to 40 cm and a diameter of 4 cm, found at depths of up to 20 m typically growing on the crests and sides of reefs, attaching to rock, and protruding sideways from

vertical surfaces[29,30]. It is known for its production of diverse secondary metabolites, which often act as chemical defenses against predators and microorganisms[31]. The selection of the marine sponge *A. compressa* for the biosynthesis of AuNPs is based on its unique production of bioactive secondary metabolites, such as alkaloids, ceramides, and terpenes, which are known for their antimicrobial, antiviral, and insecticidal properties. Marine sponges, unlike terrestrial plants, are exposed to extreme marine conditions that promote the biosynthesis of structurally diverse and potent compounds[32,33]. The objective of this study was to evaluate the antibacterial, antioxidant, anti-inflammatory, anti-biofilm, and insecticidal activities of AuNPs biosynthesized using the marine sponge *A. compressa*, with potential applications in biomedical and environmental sectors.

Materials and methods

materials

Chloroauric acid trihydrate ($HAuCl_4 \cdot 3H_2O$), sourced from Sigma-Aldrich in Egypt, was used as the gold precursor for nanoparticle synthesis. Analytical-grade chemicals, culture media, and reagents were sourced from Hi-media Co. (Egypt) and used without further purification. All biological experiments were conducted using deionized and sterilized water.

Preparation of A. compressa extract

Fresh specimens *A. compressa* were collected from the Red Sea by scuba diving at a depths of up to 20 m typically growing on the crests and sides of reefs, attaching to rock, and protruding sideways from vertical surfaces[29,30], along the El-Ahiaa region at Hurghada City. The El-Ahiaa region lies directly in the front of National Institute of Oceanography and Fisheries (NIOF) at 200 m off shore and 5 km northern Hurghada City, at latitudes 576,628 E and 577,260 E and longitudes 3,018,187 N and 3,018,384 N. Identification of specimens was carefully done on the basis of morphological characteristics By experts according to Systema Porifera [34] and the World Porifera Database[35]. The samples were rinsed three times with deionized water and air-dried. The dried material was ground using a blender and passed through a 20-mesh sieve to obtain a fine powder. A quantity of 5 g of the powder was mixed with 100 mL of distilled water and boiled at 80 °C for 1 h on a hot plate. The liquid extract was then collected from the combination by vacuum-filtering it using Whatman No. 1 filter paper[36]. As illustrated in Fig. 1, 200 mL of sterilized distilled water was added to the extract, which was then stored in an amber container at 4 °C for subsequent use.

Biosynthesis of AuNPs using *A. compressa*

To initiate the synthesis of AuNPs, chloroauric acid trihydrate ($HAuCl_4 \cdot 3H_2O$; 2.36 g, equivalent to 30 mM) was added to 200 mL of the *A. compressa* aqueous extract. Subsequently, the conditions were optimized by setting the pH to 7.2, the incubation temperature to 30 °C, and the reaction time to 24 h, with constant agitation at 150 rpm in a shaking incubator, to maximize the production of AuNPs[37]. A distinct color shift from yellow to purple indicated the formation of AuNPs. The resulting nanoparticles were harvested by centrifugation at 8000 rpm for 15 min and subsequently washed three times with deionized water to remove unbound biomolecules and residual reactants.

Characterization of AuNPs

The AuNPs synthesized under optimized conditions were comprehensively characterized using a suite of analytical techniques. UV–Vis spectrophotometry was employed to confirm the formation of AuNPs via detection of the characteristic surface plasmon resonance (SPR) peak within the range of 400–800 nm, using a Jenway 6305 Spectrophotometer (Jenway, Staffordshire, UK)[38]. The morphological features of the nanoparticles were examined through scanning electron microscopy (SEM) using a Vega3 Tescan system (Czech Republic). For SEM sample preparation, a thin film of the nanoparticle solution was deposited onto a carbon-coated copper grid, followed by drying under a mercury lamp for 5 min. Transmission electron microscopy was further used

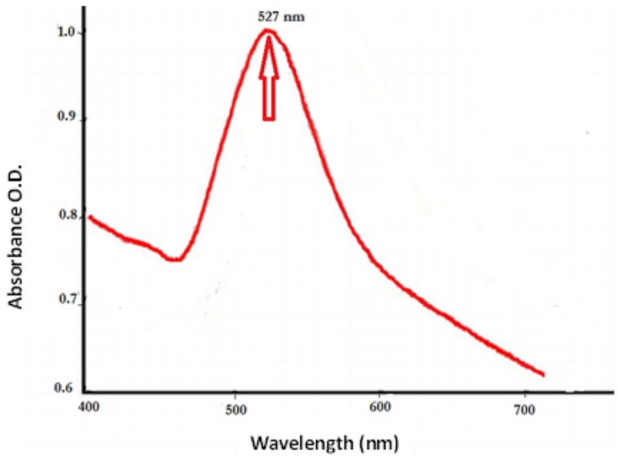

Fig.1. Biosynthesized AuNPs' SPR utilizing *A. compressa*.

to evaluate the internal structure and size distribution of the AuNPs. A droplet of the sample was placed onto a Formvar-coated copper grid and air-dried before imaging with a JEOL JEM 3010 microscope (Tokyo, Japan) at an accelerating voltage of 200 kV. Fourier-transform infrared (FTIR) spectroscopy was performed to identify functional groups in the biosynthesized nanoparticles. This analysis was conducted with a Perkin-Elmer FTIR-1600 (Waltham, MA, USA). The sample was mixed with potassium bromide and compressed into thin discs. Spectra were recorded in the range of 400–4000 cm^{-1}[39]. The crystalline structure of the AuNPs was characterized using XRD analysis. The measurements were taken with an X'Pert Pro X-ray diffractometer (Philips, Eindhoven, The Netherlands) across a 2θ range from 4° to 80°. The Debye–Scherrer equation was applied to estimate the average particle size[40]:

$$D = K\lambda/\beta Cos\theta \quad (1)$$

where,

D is the average particle size, *K* is Scherrer's constant (0.9), λ is the X-ray wavelength, β is the full width at half maximum (FWHM) of the diffraction peak, and θ represents Bragg's angle.

Biological activities

Antimicrobial activity

The antimicrobial efficacy of the biosynthesized AuNPs was assessed against a range of human pathogenic microorganisms, including *Escherichia coli* and *Klebsiella pneumoniae*, as well as *Staphylococcus aureus* and *Staphylococcus haemolyticus*. All bacterial strains were obtained from the Regional Center for Mycology and Biotechnology, Cairo, Egypt. The agar well diffusion method was employed, following the Clinical Laboratory Standards Institute (CLSI) guidelines (document M51-A2) with minor modifications[41].

Briefly, bacterial cultures were grown on nutritional agar for twenty-four hours at 37°C. Next, uniformly distribute bacterial suspensions at a concentration of 1.5×10^6 CFU/mL onto sterile Petri plates filled with Mueller–Hinton agar. Wells were then punched into the agar using a sterile cork borer (6 mm diameter), and each well was loaded with 100 µL of either the AuNP solution (500 µg/mL), the A. compressa extract, or cefuroxime (as a positive control). The plates were initially refrigerated for 2 h, followed by a 24-h incubation period at 37°C.

Determination of minimum inhibitory concentrations (MICs)

The antimicrobial effectiveness of AuNPs was further assessed using the broth microdilution technique against a variety of bacteria, including *E. coli, K. pneumoniae, S. aureus*, and *S. haemolyticus*. Serial dilutions of AuNPs were prepared in concentrations ranging from 2 to 512 µg/mL. For each concentration, 100 µL of the AuNP solution was added to 100 µL of double-strength Mueller–Hinton (MH) broth in sterile 96-well microtiter plates. Subsequently, 20 µL of bacterial suspension, adjusted to match the turbidity of the 0.5 McFarland standard, was added to each well, except for the negative controls. Positive control wells received only the bacterial solution to verify the MH broth's capacity to support bacterial growth. To assess bacterial viability, 30 µL of resazurin solution (0.002 g resazurin dissolved in 10 mL of distilled water, filtered through a 0.2 µm Millipore membrane, and stored at 4 °C for up to two weeks) was added to each well after the initial setup. The plates were then incubated at 37 °C for 24 h. The experiment concluded by measuring the optical density at 595 nm to ascertain the percentage of bacterial cell death[42].

$$\text{Percentage of bacterial inhibition} = [(\text{OD control} - \text{OD treatment})/\text{OD control}] \times 100 \quad (2)$$

The minimum inhibitory concentration (MIC) for each sample was established by identifying the smallest amount of the sample necessary to inhibit 80% of the bacterial strains' growth.

All antimicrobial assays, including agar well diffusion and MIC determinations, were performed in triplicate (n = 3) to ensure reproducibility of the results.

Anti-inflammatory activity

Preparation of erythrocyte suspension

Three milliliters of fresh whole blood were obtained from one healthy, consenting adult volunteer and collected in heparinized tubes. Then, it was centrifuged at 3000 rpm for 10 min. The supernatant was discarded, and the red blood cell pellet was resuspended in an equivalent volume of normal saline. The resulting volume was then accurately measured and reconstituted into a 40% (v/v) suspension using an isotonic buffer solution, which consisted of 10 mM sodium phosphate buffer at pH 7.4. This buffer was prepared by dissolving 0.2 g of NaH_2PO_4, 1.15 g of Na_2HPO_4, and 9 g of NaCl in one liter of distilled water. The resulting suspension of red blood cells was then utilized as prepared[43]. The study involving human blood samples was approved by the Faculty of Science Research Ethics Board under the reference number FSR 15,162,118, and all procedures were conducted in accordance with institutional ethical guidelines.

Hypotonicity induced hemolysis

For this experiment, extracts were dissolved in distilled water to form a hypotonic solution. This solution, in volumes of 5 mL and containing varying concentrations of the extracts (100, 200, 400, 600, 800, and 1000 µg/mL), was dispensed into centrifuge tubes in duplicate for each concentration. An isotonic solution containing the same extract concentrations (100 to 1000 µg/mL) was similarly prepared and dispensed into centrifuge tubes in duplicate for each dose. Control groups consisted of tubes with 5 ml of distilled water and tubes with 5 ml of a 200 µg/mL indomethacin solution, respectively. To each tube, 0.1 ml of the erythrocyte suspension was added, and the contents were gently mixed. The mixtures were centrifuged at 13,000 rpm for three minutes after an hour

of incubation at room temperature (37°C). A Spectronic (Milton, Roy) spectrophotometer was used to measure the absorbance of hemoglobin in the supernatant at 540 nm. Assuming that 100% of the hemolysis was induced by distilled water, the percentage of hemolysis was computed. The following computation was used to assess the extract's ability to prevent hemolysis[44]:

$$\% \text{ Inhibition of hemolysis } = 1 - ((OD2 - OD1) / (OD3 - OD1)) * 100$$

where OD1 represents the test sample's absorbance in an isotonic solution, OD2 represents the test sample's absorbance in a hypotonic solution, and OD3 represents the control sample's absorbance in a hypotonic solution.

In vitro biofilm inhibition activity

The microtitre plate (MTP) method, with slight adjustments, was employed to explore the potential of AuNPs in inhibiting or reducing biofilm formation by clinical strains of *S. aureus* and *Pseudomonas aeruginosa*, the latter being known for its significant biofilm-producing capabilities[45]. In brief, tryptic soy broth (TSB) was supplemented with 1% glucose and mixed with various concentrations of AuNPs in a flat-bottomed MTP. After being diluted 1:100 for overnight, the test organisms were added to the MTP and incubated for 48 h at 37°C, resulting in an inoculum size of 1.5×10^8 CFU/ml. Using spectrophotometry, the growth density was determined at an optical density (OD) of 620 nm. Subsequently, planktonic cells were gently aspirated from all MTP wells to avoid disrupting the already formed biofilm. Three washes of phosphate-buffered saline (PBS) at pH 7.4 were performed on the wells to remove any remaining detached cells. In each well, 200 µL of 95% methanol was added to fix the biofilm. Once the biofilms were stained, 200 µL of 0.3% Crystal Violet (CV) was added, and the plates were then incubated for 15 min at 20–25 °C. Sterile distilled water was then used to carefully remove any remaining CV solution. Next, using an Olympus C K40 inverted microscope at 150 × magnification, the biofilm-bound CV stain was inspected and photographed. Biofilm formation was quantitatively analyzed by adding 200 µL of 30% acetic acid to each well. The absorbance at 540 nm was measured using a Tecan Elx800 microplate reader[46]. To assess treatment efficacy, the results from treated and untreated wells were compared.

Evaluation of antioxidant activity using the DPPH radical scavenging method

The scavenging ability of free radicals by different extracts of *A. compressa* was assessed through the 1,1-diphenyl-2-picrylhydrazyl (DPPH) assay[47]. A 0.1 mM DPPH solution in ethanol was prepared, and 1 ml of this solution was combined with 3 ml of various *A. compressa* extract concentrations in ethanol (ranging from 3.9 to 1000 µg/ml). It's important to note that only extracts soluble in ethanol were used, and their concentrations were meticulously prepared through dilution. After vigorous shaking, the mixtures were allowed to stand at room temperature for 30 min. Next, a UV–VIS spectrophotometer (Milton, Roy) was used to detect the absorbance at 517 nm. Ascorbic acid served as the reference standard, and the procedures were performed three times. Based on the log-dose inhibition curve, the IC_{50} value which represents the dosage required to inhibit 50% of the DPPH radicals was determined. A greater free radical scavenging effect is indicated by a lower absorbance value of the reaction mixture. The following formula was used to determine the percentage of DPPH scavenging effect[48]:

$$\text{DPPH scavenging effect } (\%) \text{ or Percent inhibition } = \text{A0} - \text{A 1} / \text{A0} \times 100$$

where A1 represented the absorbance while the test or standard sample was present, and A0 represented the absorbance of the control response.

Colonization of tested insects

Maintenance of the House fly colony

The department of entomology at the faculty of science at Ain Shams university in Egypt generously provided the housefly, *(Musca domestica)* maggots from a laboratory-maintained susceptible strain. The colony was reared for several generations under controlled conditions of 27 ± 2 °C and 65 ± 10% relative humidity. A mixture of 38 g of sterilized bran, 2 g of milk powder, and 60 ml of water was used as a rearing medium. Pupae were gathered and moved to new cages that were furnished with autoclaved cotton soaked in 10% w/v milk powder for the purpose of providing nourishment for adults and oviposition Sawicki (1964). The freshly laid eggs were moved to glass beakers that were filled with food to aid in the larval development and hatching.

Mosquitoes colony

The *Culex pipiens* mosquito utilized in this study was collected from colony maintained at the Faculty of Science, Tanta University, Egypt. After that, larvae were raised for two more generations under a14–10 h of day and night photoperiod conditions at 27 ± 2 °C and 75 ± 5% relative humidity (RH). They were fed fish meal as needed. The pupae that were produced were placed in cups with dechlorinated water in them. A piece of sponge soaked in a 10% sugar solution was given to the adults.

Bioassay

House fly adulticidal activity

With minor adjustments, the topical application method as outlined by Mansour et al.[49] was utilized to conduct the adulticidal bioassay for *M. domestica*. Ten three-day-old adult houseflies were randomly selected and anesthetized with diethyl ether for five minutes. As a result, the adults' dorsal thorax may be injected with one microliter of test solutions using a Hamilton microliter syringe 701-N (Sigma-Aldrich). Dimethyl sulfoxide (DMSO) was used as the negative control and cypermethrin (Dethriod 10*, 10% w/v cypermethrin, Pentacheme

Co. Ltd., Thailand) as the positive control at a dosage of 1 µL/adult. For both the crude and AuNPs extracts, a range of concentrations (5 – 60 µL/adult) and (4 – 20 µL/adult) were utilized to calculate the LC50 and LC90 values, respectively. A 0.1% DMSO solution was used to dissolve the crude extract, and an equal amount was added to the control. Every treatment was kept in a 500 ml glass beaker with muslin cover for a full day at 28 ± 2 °C. The cotton piece used for the incubation was autoclaved and soaked in milk powder to serve as food. Three copies of each treatment were made. 24 h after treatment, the mortality rate of the treated flies was determined using the following formula: Mortality (%) = {A-B/A} × 100, where (A) is the proportion of adults who made it out of the control groups and (B) is the proportion of people who made it out of the treatment groups.

Mosquitoes adulticidal activity

According to the World Health Organization's standard tube bioassay method [50], adulticidal activity was estimated. Ten female mosquitoes were removed from the colony and placed into holding tube for one hour. After that, the mosquitoes were carefully moved to the exposure tube for a further hour, where Whatman filter papers No. 1 (10 × 10 cm) were used to apply the crude and AuNPs. Tempephos (1 ppm) was utilized as a positive control, and papers treated with Ac AuNPs dissolved in 0.1% DMSO solution were given to the negative control group. For the examined extracts, a range of concentrations from 1 to 20 ppm were evaluated. The mosquitoes were given a piece of cotton soaked in a 10% sucrose solution to place on top of the mesh net after the exposure time and were then gently returned to the holding area, where they had been left for twenty-four hours. Each concentration was tested in triplicate. Mortality was recorded 24 h post-exposure.

Fecundity and egg-hatchability of M. demostica

Equal numbers of male and female house flies, along with the control, that survived treatment at various tested concentrations were moved to 500 ml glass beakers covered in mesh net (some concentrations were excluded from this experiment due to small or no sample size). Cotton pieces soaked in 10% w/v milk powder were used as adult food in glass beakers, and petri plates with diet (25 g coarse wheat bran) were used as a substrate for egg deposition. Every day, deposited eggs were meticulously gathered. Fecundity was then determined by dividing the total number of eggs deposited by the number of females who mated and lived to the conclusion of the experiment. Egg-hatchability % was computed as follows, whereas mean egg-hatchability was determined by dividing the total number of hatched eggs by the number of females who were successful in depositing eggs. Egg-hatchability (%) = A/B × 100, where (A) is the number of hatched eggs and (B) is the number of deposited eggs [51].

Fecundity and egg-hatchability of C. pipiens

To find out how the tested materials affected the fertility and egg-hatchability of the female Culex pipiens mosquitoes, an equal number of male and female mosquitoes that survived and emerged from treatments were allowed to mate normally (in conventional cages) alongside the control. The number of eggs laid by a female was recorded and quantified using the method outlined by Rak and Ishii[52]. Fecundity and hatchability percentages were calculated in the same manner as for houseflies.

Statistical analysis

Excel 365 was used to enter data. For every category, descriptive statistics were computed, which included the mean and standard error (SE). Adult mortality was calculated using regression, LC_{50}, and LC_{90} with 95% confidence limits using probit analysis. Using SPSS version 29, Chi-square values, lower and upper confidence limits, and one-way analysis of variance were carried out. Pairwise comparisons were performed with the Holm Sidak post hoc method. The data was displayed as Mean ± SE, and a P value of less than 0.05 was deemed significant.

Results

Characterization of AuNPs

The transition in the color of the synthesized AuNPs, changing from yellow to purple, is depicted in Figure S1. This color shift reflects the successful formation of AuNPs, attributed to their surface plasmon resonance properties.

As shown in Fig. 1, the UV–Vis analysis of the AuNPs displayed a distinct absorption peak at 527 nm. This peak corresponds to the SPR, indicating the successful synthesis and stability of the nanoparticles.

Fig. 2The FTIR spectrum of the synthesized AuNPs exhibited distinct stretching bands at 3273, 2929, 2039, 1600, 1374, 1046, 784, 504, and 435 cm^{-1}, each corresponding to specific functional groups involved in the synthesis and stabilization process. The broad band at 3273 cm^{-1} is assigned to O–H stretching vibrations, indicating the presence of phenolic compounds, flavonoids, and benzophenones in the *A. compressa* extract. These compounds likely contribute to the reduction of gold ions and act as natural stabilizers. The peak at 2929 cm^{-1} may correspond to C–H stretching vibrations of aliphatic chains. The band at 2039 cm^{-1}, although less commonly reported, could be associated with C≡C or C≡N stretching, suggesting the presence of minor alkyne or nitrile groups. A sharp peak at 1600 cm^{-1} corresponds to aromatic C = C stretching, confirming the existence of aromatic ring systems. The 1374 cm^{-1} peak is attributed to N–O stretching in nitro compounds, while the 1046 cm^{-1} band indicates C–O stretching, typically associated with alcohols, ethers, or esters that may function as capping agents. Additionally, the 784 cm^{-1} band represents C–H bending vibrations, characteristic of alkanes. The low-frequency bands at 504 cm^{-1} and 435 cm^{-1} are indicative of metal–ligand interactions, likely involving Au–O or Au–C bonds, supporting the successful formation and stabilization of gold nanoparticles.

The XRD pattern of the *A. compressa*-mediated gold nanoparticles revealed a crystalline structure, highlighted by an intense peak confirming the face-centered cubic (fcc) nature of the AuNPs (Fig. 3). This structure was evidenced by peaks at angles 37.09°, 44.28°, 65.01°, and 77.83°, corresponding to the (111), (200), (220), and

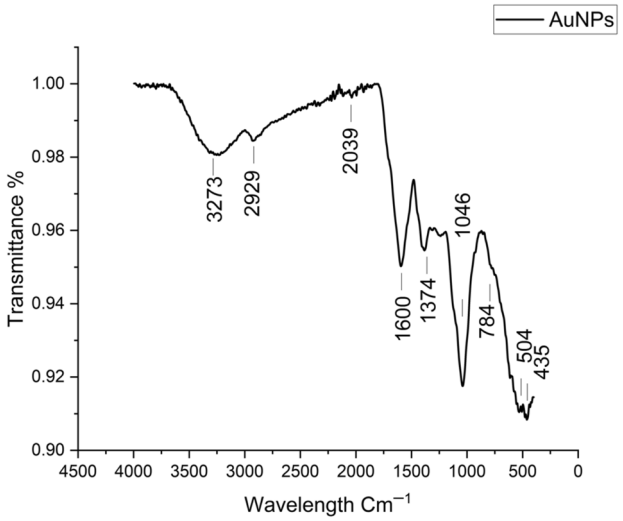

Fig. 2. FTIR analysis of biosynthesized AuNPs by using *A. compressa*.

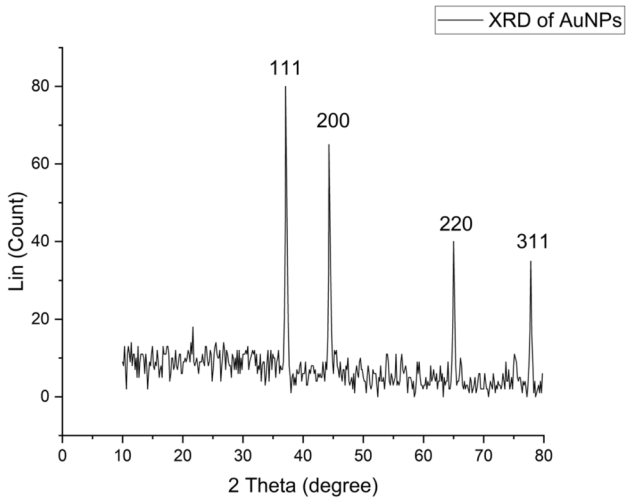

Fig. 3. XRD analysis of biosynthesized AuNPs.

(311) planes, respectively. The observed data were then compared with the standard reference from the JCPDS file (No. 00–004–0784). X-ray diffraction (XRD) analysis of the biosynthesized AuNPs revealed a prominent peak at $2\theta = 37.09°$, corresponding to the (111) plane of face-centered cubic (fcc) gold. The average crystallite size of the nanoparticles was calculated using the Debye–Scherrer equation, based on the full width at half maximum (FWHM) of 0.5° and an X-ray wavelength of 0.25719 nm. The estimated average crystallite size was found to be 29.21 nm, indicating the nanoscale crystalline nature of the synthesized particles. This result is consistent with the particle size range (10–40 nm) obtained from TEM analysis.

The TEM image in Fig. 4A reveals that the synthesized AuNPs predominantly exhibit spherical to oval in shape, with sizes ranging between 10 to 40 nm. These particles display uniformity in both shape and size. In addition, the SEM analysis, depicted in Fig. 4B, provides further insight into the morphology of the AuNPs prepared using *A. compressa* extract. The SEM analysis illustrates aggregated nanoparticles, forming distinct flower-like clusters and spindle-shaped assemblies. This aggregation suggests strong interactions between the particles, possibly due to their stabilization by bioactive compounds in the extract.

Biological activity

Antibacterial activity

The antibacterial activity of the green-synthesized AuNPs was evaluated against both Gram-positive and Gram-negative bacterial strains using the agar well diffusion method. These AuNPs demonstrate notable antibacterial efficacy, against four bacterial strains by interacting with a significant number of bacteria and subsequently destroying them. According to the results presented in Figs. 5, there was a noticeable increase in the inhibition zones for *E. coli* and *K. pneumoniae* when compared to Gram-positive bacteria. This indicates that the AuNPs,

synthesized utilizing *A. compressa* extract, showed superior antibacterial activity against Gram-negative bacteria. The negative control displayed no zones of inhibition on the agar plates, but the positive control shows moderately high inhibition zone against *E. coli, K. pneumoniae* and *S. aureus* and low inhibition zone against *S. haemolyticus*. Drawing from the data gathered, the MIC necessary to inhibit the proliferation of microorganisms was determined to be 32 µg/ml for *S. aureus* and *S. haemolyticus*. However, for *E. coli* and *K. pneumoniae*, the MIC was identified as 16 µg/ml, as illustrated in Fig. 6.

Antibiofilm activity

The synthesized AuNPs exhibited notable anti-biofilm activity against four multi-drug resistant (MDR) bacterial strains, outperforming the positive control samples. As shown in Fig. 7, the highest anti-biofilm effect was observed against *S. aureus* with a value of 2.290, followed by *S. haemolyticus* at 1.880, *E. coli* at 1.425, and *K. pneumoniae* at 1.120. These results highlight the potential of AuNPs in disrupting biofilm formation, especially in drug-resistant bacterial infections.

Anti-inflammatory activity

The anti-inflammatory activity in vitro was assessed through methods of protein denaturation and hemolysis of HRBC membranes, chosen due to the similarity between erythrocyte and lysosomal membranes. The green-synthesized AuNPs were tested for their anticoagulant properties as well, demonstrating negligible hemolytic effects on RBCs. Various concentrations of AuNPs (1000, 800, 600, 400, 200, and 100 µg/mL) were examined, with the hemoglobin absorption measured at 540 nm spectroscopically. The recorded hemolytic inhibition percentages were 4.8, 10.2, 12.8, 14.9, 19.5, and 22.4%, respectively. These figures were lower compared to those listed in (Table 1).

Antioxidant activity

The concept of antioxidant activity involves the use of antioxidants to prevent the start of oxidative chain reactions by producing non-reactive radicals. This study explored the antioxidant abilities of the *A. compressa*

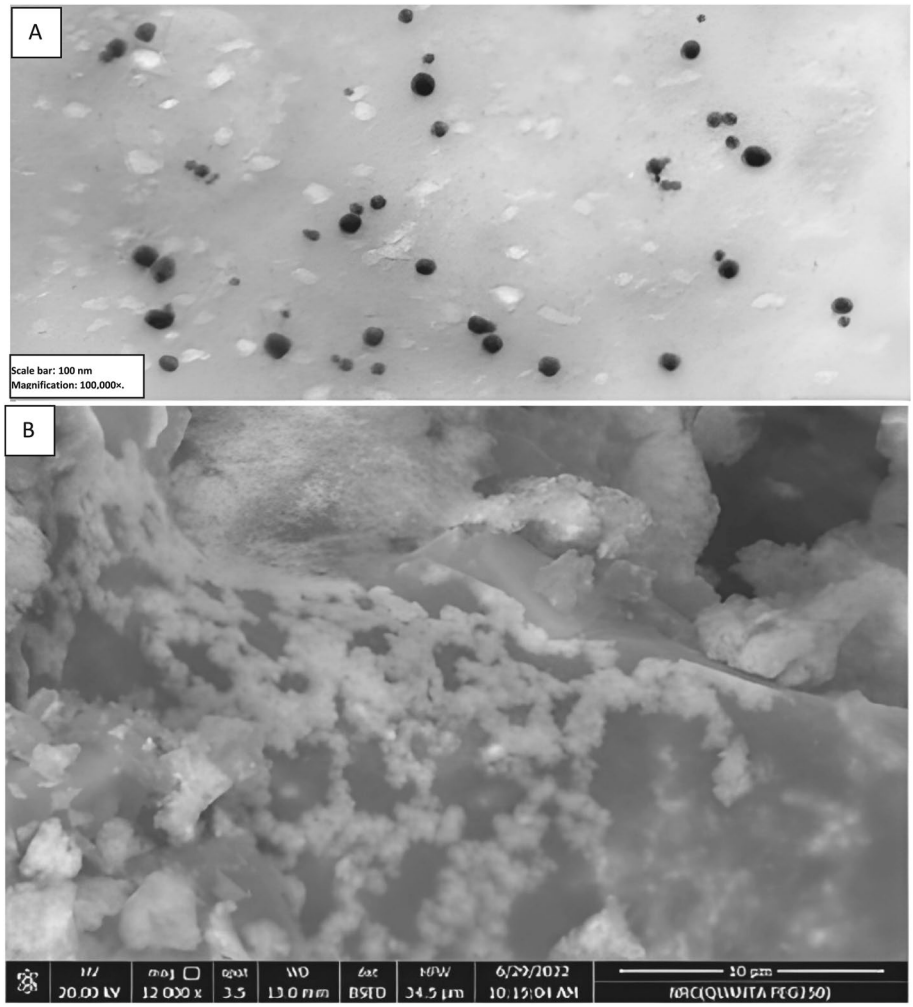

Fig. 4. **A**) TEM analysis and **B**) SEM image of biosynthesized AuNPs.

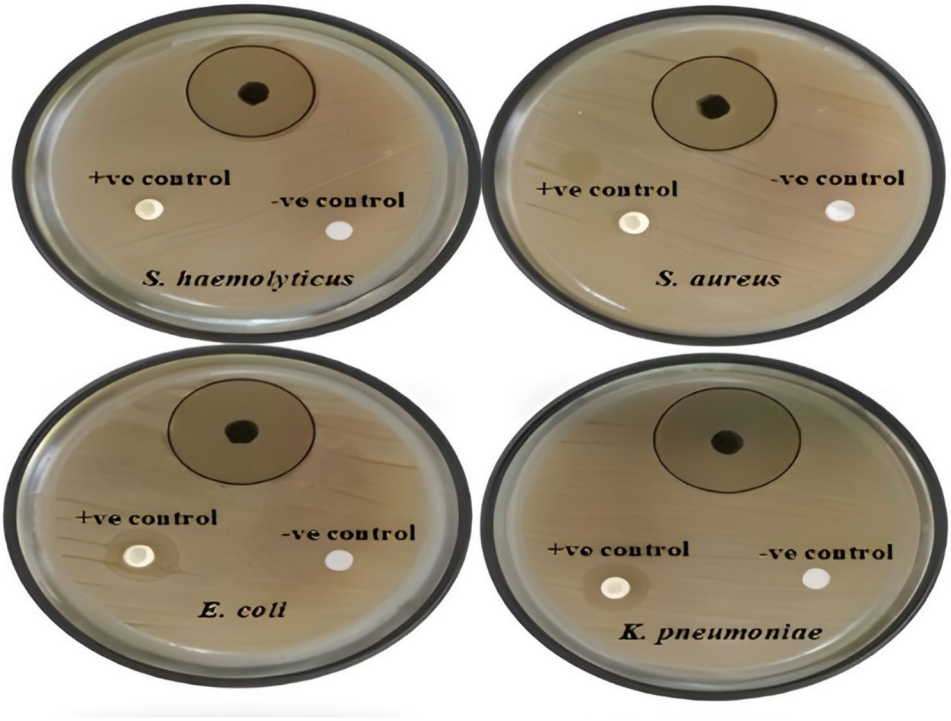

Fig. 5. Antibacterial activity of biosynthesized AuNPs, at a concentration of 500 µg mL^{-1}. Where, negative control is *A. compressa* extract and positive control is cefuroxime.

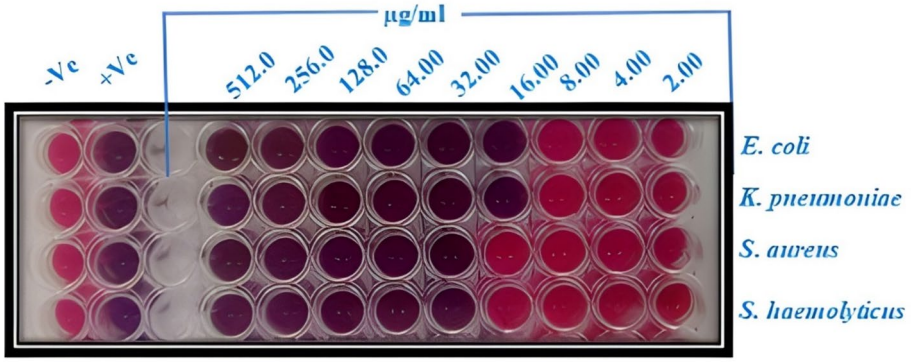

Fig. 6. Minimum inhibitory concentrations and minimum lethal concentrations of different bacterial strains by Resazurin technique.

extract in water, AuNPs, and controls using DPPH assays. The capacity to neutralize DPPH was measured against ascorbic acid, a known standard, with results detailed in Table 2. The AuNPs demonstrated significant DPPH neutralization at rates of 92.5, 85.5, 78.7, 71.7, 64.7, 57.8, 51.1, 44.4, 38.1, and 31.4%, corresponding to a mean IC50 value of 13.54 µg/mL across varying concentrations (1000, 500, 250, 125, 62.5, 31.25, 15.625, 7.8125, 3.9, and 1.95 µg/mL). Despite this, these figures were significantly lower than those for ascorbic acid, which had an IC50 of 3.45 µg/mL. The raw *A. compressa* extract, with an IC50 of 27, was more effective than AuNPs but less so than ascorbic acid at identical concentrations (as illustrated in Table 2).

Insecticidal properties against diseases vectors

The house fly treated with five doses for both crude and synthesized AuNPs (5, 15, 30, 45,and 60 µL/adult) and (4, 8, 12, 16, and 20 µL/adult)), respectively, showed high adulticidal activity against adult and It became crystal clear when recorded LC50 and LC90 values of both crude and synthesized AuNPs were (34.988 and 62.836 µL/adult) and (8.545 and 15.157 µL/adult), respectively. Adult mortality reached 93.33% at 60 µL/adult of crude extract while reached the same concentration (100%) at 20 µL/adult of AuNPs extract (Table 3). In the same context *culex pipiens* mosquito treated with five concentration for both crude and synthesized AuNPs (2.5, 5, 10, 15,and 20 ppm) and (1, 2, 4, 8,and 16 ppm) , respectively, showed high Adulticidal activity against where

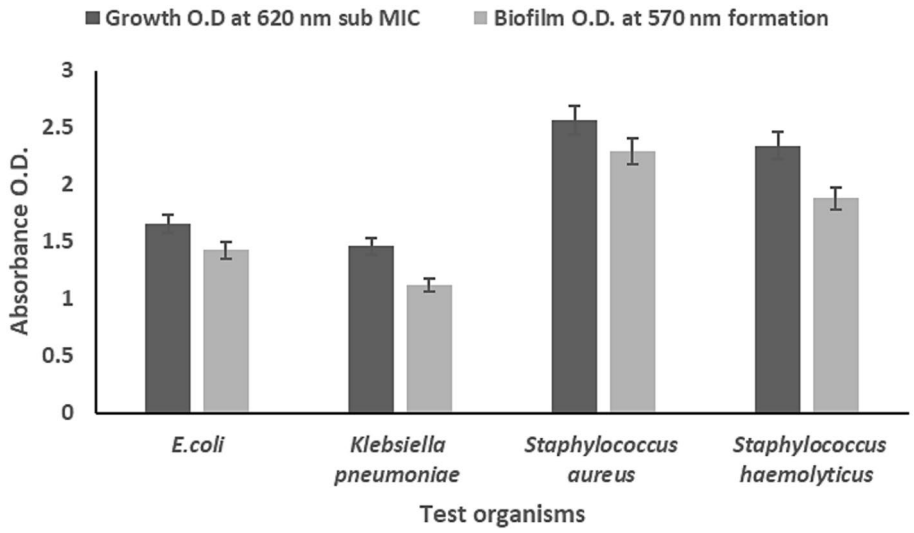

Fig. 7. Anti-biofilm formation activity of AuNPs against four MDR isolates. Means are significantly different at $p < 0.05$.

Concentrations (µg/mL)	Anti-inflammatory —AuNPs	Anti-inflammatory —Indo	Hemolysis inhibition %— AuNPs	Hemolysis inhibition %— indo
Control	1.972	1.972	**0**	**0**
1000	0.135	0.027	95.2	99.6
800	0.225	0.056	89.8	97.8
600	0.272	0.076	87.2	96.5
400	0.307	0.092	85.1	95.5
200	0.393	0.103	80.5	94.8
100	0.446	0.115	77.6	94.2

Table 1. Anti-inflammatory effects of different AuNP concentrations against reference accompanied by low hemolytic activity.

DPPH scavenging%			
Concentration (µg/mL)	A. *compressa* extract (µg/mL)	Ascorbic acid (µg/mL)	AuNPs (µg/mL)
1000	94.1 ± 0.81^{a}	95.5 ± 0.31^{a}	92.5 ± 0.51^{a}
500	90.2 ± 0.31^{a}	92.9 ± 0.51^{a}	85.5 ± 0.21^{b}
250	90.1 ± 0.41^{a}	91.1 ± 0.81^{a}	78.7 ± 0.81^{c}
125	88.7 ± 0.51^{b}	84.9 ± 0.81^{b}	71.7 ± 0.71^{c}
62.5	77.1 ± 0.83^{c}	76.4 ± 0.81^{c}	64.7 ± 0.71^{d}
31.25	70.2 ± 0.81^{c}	69.6 ± 0.93^{d}	57.8 ± 0.79^{e}
15.625	66.1 ± 0.91^{d}	62.6 ± 0.84^{d}	51.1 ± 0.81^{e}
7.8125	53.5 ± 0.73^{e}	54.7 ± 0.88^{e}	44.4 ± 0.96f.
3.9	42.8 ± 0.99f.	44.3 ± 0.91^{g}	38.1 ± 1.01^{g}
1.95	40.3 ± 1.21f.	40.2 ± 1.01^{h}	31.4 ± 1.11^{g}
0	0 ± 0.0	0 ± 0.0	0.0 ± 0.0

Table 2. DPPH free radical scavenging activity of *A. compressa* extract, AuNPs, and ascorbic acid as reference at different concentrations. Mean ± SE of three replicates, means in the same column followed by different letters differ significantly, $P < 0.05$.

recorded LC50 and LC90 values of both crude and synthesized AuNPs were (9.258 and 17.399 ppm) and (7.573 and 14.074 ppm), respectively. Adult mortality reached 96.67% at 20 ppm of crude extract while reached (100%) at 16 ppm of AuNPs extract (Table 4). Generally, *M. domestica* and *C. pipiens* mosquito were found to be more sensitive to our AuNPs than crude extract.

In addition to adulticidal effects, fecundity and egg hatchability of both *M. domestica* and *C. pipiens* declined significantly with increasing concentrations of both crude and AuNPs treatments. For *M. domestica*, these effects were observed at 60 µL/adult (crude) and 12 µL/adult (AuNPs), as shown in Table 5. Similarly, for *C. pipiens,* fecundity and hatchability reductions were noted at 20 ppm (crude) and 16 ppm (AuNPs) (Table 6). Notably, the AuNPs exhibited a more pronounced inhibitory effect on reproductive parameters than the crude extract, indicating enhanced bioefficacy of the synthesized nanoparticles.

Discussion

The eco-friendly production of AuNPs has captivated researchers due to their vast importance in fields like nano-optics, nano-sensors, nano-catalysis, and nanomedicine. Utilizing green technology to synthesize AuNPs offers several advantages over chemical methods, including environmental sustainability and cost-efficiency [53]. Various plants and algae have proven to be efficient sources for reducing $HAuCl_4{\cdot}3H_2O$ into AuNPs. In the present study, we employed the extract from *A. compressa* as a reducing agent to synthesize AuNPs. A characteristic color change of the reaction mixture from yellow to purple signified the formation of AuNPs, attributable to SRP. Similar visual indicators of AuNP formation have been reported in other studies. For example, *Sargassum serratifolium* extract facilitated the rapid synthesis of SS-AuNPs, with the colloidal solution turning violet within 15 min, indicating nanoparticle formation[54]. Likewise, Donga et al. [55], the application of *M. indica* seed extract for the production of AuNPs was first evidenced by a swift shift in the solution's color from transparent to a purplish-red within just 5 min, indicating the formation of AuNPs. As the duration of incubation increased, the solution's color intensity grew due to the enhanced synthesis of AuNPs, ultimately reaching a deep purple-red shade after 24 h. Conversely, AuNPs production with microalgae extracts (*chlorella*) and cyanobacteria (*spirulina*) resulted in a ruby-red colored solution, as reported by Zayadi and Bakar,[56]. Similarly, Amina et al.[57], achieved the synthesis of AuNPs using algal extract from *Dictyosphaerium* sp., with the reaction yielding a ruby-red solution. Consistent with this observation, Mariychuk et al.[58], stated that the AuNPs synthesized using *Mentha piperita* L. extract also produced a ruby-red solution. Kamaraj et al.[59], further noted that the biosynthesis of AuNPs using *Gracilaria crassa* leaf extract resulted in a ruby-red colored solution. Shah et al.[60] employed *Sageretia thea* leaf extract as a reducing, stabilizing, and capping agent, observing the formation of ruby-red colloidal AuNPs. In comparison, Borse and Konwar[61] synthesized gold nanoparticles using trisodium citrate as a chemical reducing agent, resulting in a reddish-purple colloidal suspension. Additionally, Clarance et al.[62] reported that biosynthesis of AuNPs using the endophytic fungus *Fusarium solani* produced color transitions ranging from pink to ruby-red. These distinct color changes are indicative of SPR phenomena and reflect alterations in the oxidation state of gold ions during nanoparticle formation.

Due to SPR, AuNPs exhibit absorbance in the UV–Visible spectrum. Notably, the location of the absorption maxima provides insights into the nanoparticles' morphology. In the current study, the absorption peak appeared at a comparatively lower wavelength of 527 nm, indicative of the smaller size of the synthesized AuNPs. This observation is consistent with the findings of Kim et al.[54] who reported a peak at 528 nm. Similarly, Pitchai et al.[63] documented an absorption maximum at 540 nm for their synthesized AuNPs, while Clarance et al.[62] noted that spherical AuNPs typically exhibit SPR peaks within the 510–560 nm range. Another study found the absorption peak of AuNPs at 533 nm when using *Andrographis paniculata* leaf extract, as reported by Paramasivam et al.[64]. Rokkarukala et al.[65], observed that the initial evidence of SCE-AuNP (AuNPs synthesized using a specific extract) formation was the alteration in the reaction medium's color from a light yellowish tint to dark violet

Treatments	Concentrations µL/adult	*n*	Adult mortality (%)	Regression equation	LC_{50} (LCL–UCL) (µL/adult)	LC_{90} (LCL–UCL) (µL/adult)	χ^2
Crude extract	Control	30	0.0 ± 0.0^{a}	Y = 1.445X—0.7953	34.988 (16.707—53.269)	62.836 (49.414—84.344)	2.437 n.s
	5	30	13.34 ± 0.59^{a}				
	15	30	20.0 ± 2.32^{a}				
	30	30	33.54 ± 3.46^{ab}				
	45	30	60.0 ± 2.32^{be}				
	60	30	93.33 ± 4.77^{cbe}				
Nano Extract	Control	30	0.0 ± 0.0^{a}	Y = 5.4167X + 1.6667	8.545 (4.609—11.481)	15.157 (13.944—19.706)	1.069 n.s
	4	30	16.67 ± 0.27^{ab}				
	8	30	46.34 ± 0.81^{bd}				
	12	30	73.33 ± 1.27^{cd}				
	16	30	96.67 ± 2.58^{c}				
	20	30	100.0 ± 0.0^{c}				
Cypermethrin	1	30	100.0 ± 0.0				

Table 3. Adulticidal activity of crude and synthesized AuNPs extracts against the house fly, *M. domestica*. (LC_{50}) concentration that kills 50% of population, (LC_{90}) concentration that kills 90% of population, (LCL) lower confidence limit, (UCL) upper confidence limit, χ^2 Chi-square, The Holm-Sidak post hoc test was used to examine the data after a one-way ANOVA. The results were displayed as Mean ± SE of three replicates, with $P < 0.05$, n = sample size, and means in the same column denoted by distinct letters differing substantially.

Treatments	Concentrations ppm	*n*	Adult mortality (%)	Regression equation	LC_{50} (LCL–UCL) (µL/adult)	LC_{90} (LCL–UCL) (µL/adult)	χ^2
Crude extract	Control	30	0.0 ± 0.0a	Y = 4.870X – 0.947	9.258 (8.703 – 9.814)	17.399 (15.992 – 18.807)	8.863 n.s
	2.5	30	13.33 ± 3.33^{ab}				
	5	30	20.0 ± 0.0^{ab}				
	10	30	46.67 ± 8.81^{c}				
	15	30	73.33 ± 3.33^{d}				
	20	30	96.67 ± 3.33^{e}				
Nano Extract	Control	30	0.0 ± 0.0a	Y = 6.693X + 3.714	7.573 (4.966 – 10.179)	14.074 (12.665 – 15.481)	10.553 n.s
	1	30	3.33 ± 3.33^{a}				
	2	30	6.67 ± 3.33^{a}				
	4	30	46.67 ± 3.33^{b}				
	8	30	70.0 ± 0.0^{c}				
	16	30	100.0 ± 0.0^{d}				
Temephos	1	30	100.0 ± 0.0				

Table 4. Adulticidal activity of crude and synthesized AuNPs extracts against the mosquito, *Culex pipiens*. (LC_{50}) concentration that kills 50% of population, (LC_{90}) concentration that kills 90% of population, (LCL) lower confidence limit, (UCL) upper confidence limit, χ^2 Chi-square, The Holm-Sidak post hoc test was used to examine the data after a one-way ANOVA. The results were displayed as Mean ± SE of three replicates, with $P < 0.05$, n = sample size, and means in the same column denoted by distinct letters differing substantially.

Treatments	Concentrations µL/adult	Fecundity Mean ± SE	Egg-Hatchability (%)
Crude extract	Control	51.33 ± 1.86^{a}	94.04
	5	42.33 ± 0.33^{b}	83.48
	15	31.67 ± 0.67^{c}	84.19
	30	21.67 ± 1.76^{d}	39.51
	45	9.67 ± 1.76^{e}	24.58
	60	-	-
	Statistic summary	DF = 4, F = 132.554, P = 0.000	
Nano Extract	Control	52.67 ± 1.45^{a}	94.96
	4	33.33 ± 1.45^{b}	63.02
	8	23.67 ± 0.89^{c}	40.67
	12	-	-
	16	-	-
	20	-	-
	Statistic summary	DF = 2, F = 130.822, P = 0.000	

Table 5. Fecundity and egg hatchability of the adult house fly, *M. domestica* females treated with different concentrations of crude and synthesized AuNPs extracts. Data were analyzed by one-way ANOVA, followed by Holm Sidak post hoc test and presented as Mean ± SE of three replicates. For each treatment, means followed by different letters differ significantly, $P < 0.05$.

within 30 min after the extract's introduction. Results in the UV–visible spectrum, which revealed a peak at 540 nm, which corresponds to the SPR linked to the nanoparticles, supported this alteration. Variations in the wavelength and intensity of SPR bands are influenced by several parameters, including particle size, shape, metal ion concentration, the type and amount of reducing and capping agents, the nature of the plant extract, and the dielectric constant of the medium[66]. Additionally, a key factor in changing the reaction mixture's color is the SPR phenomenon, which is the collective oscillation of free electrons in metallic nanoparticles brought on by the electromagnetic field[67].

The crystallinity of the AuNPs synthesized using *A. compressa* was evaluated using XRD analysis, examining the diffraction pattern within the 2θ range of 10° to 80°. This analysis confirmed the presence of metallic Au components in the nanoparticles, aligning with findings from previous studies[54,64,68]. In a related study, Clarance et al.[62], identified the diffraction peaks at (006), (111), (200), (220), and (311) for AuNPs produced using the endophytic fungus *Fusarium solani*.

Fourier-transform infrared (FTIR) spectroscopy was employed to identify the functional groups associated with the algal-mediated synthesis of AuNPs. Prominent transmission bands were detected at 3273, 2929, 2039,

Treatments	Concentrations ppm	Fecundity	
		Mean ± SE	Egg-Hatchability (%)
Crude extract	Control	150.33 ± 6.48^{ab}	91.07
	2.5	148.0 ± 4.36^{b}	84.99
	5	125.67 ± 2.33^{c}	78.10
	10	93.33 ± 3.48^{d}	62.08
	15	61.33 ± 2.4^{e}	38.15
	20	30.33 ± 2.9f.	13.33
	Statistic summary	DF = 4, F = 153.418, P < 0.01	
Nano Extract	Control	140.0 ± 2.88^{ab}	90.51
	1	125.33 ± 3.17^{b}	75.24
	2	112.67 ± 2.18^{bc}	62.89
	4	80.0 ± 2.88^{d}	37.15
	8	29.0 ± 2.08^{e}	15.81
	16	6.0 ± 1.0f.	0.00
	Statistic summary	DF = 4, F = 480.504, P < 0.01	

Table 6. Fecundity and egg hatchability of adult female *C. pipiens* mosquitoes treated with varying doses of synthetic and crude AuNPs extracts. Data were analyzed by one-way ANOVA, followed by Holm Sidak post hoc test and presented as Mean ± SE of three replicates. For each treatment, means followed by different letters differ significantly, $P < 0.05$

1600, 1374, 1046, 784, 504, and 435 cm^{-1}, aligning with findings from El-Sheekh et al.[69] and Rokkarukala et al.[65]. This analysis demonstrated the dual function of algal bio-compounds in both reducing and capping Au-NPs, highlighting the critical role of capping agents in nanoparticle stability[70]. The investigation revealed that algal polysaccharides, proteins, and phenolic compounds, characterized by carboxylic and amine groups in proteins, are instrumental in reducing Au^{+} ions to Au^{0} and subsequent nanoparticle stabilization. Similar conclusions were drawn by Sidhu et al.[71], identified proteins, polysaccharides, and phenolic compounds as playing significant roles in stabilizing and capping nanoparticles.

Additionally, both abiotic and biotic components are implicated in the reduction process, with reducing sugars in the polysaccharide sheath and fatty acids in the plasma membrane among the abiotic factors and reducing enzymes as biotic factors[72]. It was noted that exo-polysaccharides, which are abundant in reducing sugars capable of forming nanoparticles, are produced extracellularly and may detach from cellular filaments[73]. The amount of biologically active chemicals or cell counts, as well as the concentration of metal ions, affect the creation of nanoparticles. The synthesis techniques, reducing agents, and stabilizers employed all affect the size, shape, and distribution of the nanoparticles, which in turn affects their efficiency. The reduction of metal ions is caused by the many hydroxyl groups found in algal pigments[74].

Transmission electron microscopy (TEM) serves as a critical tool for determining the size and shape of biosynthesized AuNPs[75]. In this study, we observed AuNPs ranging in size from 10 to 40 nm, predominantly spherical or oval. Folorunso et al.[76] used TEM to assess the size, structure, and dispersion of AuNPs, finding them to be sphere-shaped with an average size of 37.7 nm. Kim et al.[54] reported an average size of 7.18 nm for AuNPs in TEM images. Paramasivam et al.[64]found AP-AuNPs synthesized with *Andrographis paniculata* leaf extract to be well dispersed, sized between 10 and 50 nm, primarily spherical with a few hexangular and trilateral. El-Sheekh et al.[69], observed Au-NPs biosynthesized by blue-green algae in triangular, pentagonal, and slightly spherical shapes, with sizes ranging from 15.49 to 55.08 nm. Babu et al.[77], noted As-AuNPs as spherical with an average size of less than 20 nm, while Subbulakshmi et al.[78], reported AuNPs prepared using *Gelidiella acerosa* to be 5–20 nm in diameter and spherical. Chen et al.[79], documented Au nanoparticles synthesized by Curcumae *Kwangsiensis folium* in the size range of approximately 8–25 nm. Additionally, structural morphology was also assessed using SEM studies. Similarly, Chen et al.[79] described a wheat-like texture and, due to high sampling concentration, observed some lump-like agglomeration.

The results indicated that AuNPs were effective against all the tested bacterial strains, with a notably stronger antibacterial impact on gram-negative bacteria. This enhanced efficacy can be attributed to the structural differences between gram-positive and gram-negative bacteria; which gram-positive bacteria possess a robust cell wall, whereas gram-negative bacteria have a thinner cell wall, allowing AuNPs easier access to and subsequent damage of the cell membrane in gram-negative bacteria[80]. The mechanism behind the antibacterial properties of AuNPs involves two primary processes. Firstly, they disrupt the metabolic process by altering membrane potential and inhibiting adenosine triphosphate ATP synthase activity[81]. Secondly, they prevent the ribosome's subunit from binding to transfer RNA (tRNA), effectively impairing its biological functions. Additionally, they were found to be less toxic to mammalian cells[82,83]. Gold nanoparticles, owing to their diverse sizes and shapes, have been extensively studied for their antibacterial and anti-biofilm capabilities[84]. The small size and increased surface area of AuNPs generate electronic effects that enhance the surface reactivity, making them highly effective. Moreover, their large surface area facilitates extensive interaction with bacteria, significantly boosting antibacterial activity[85]. These properties underscore the considerable increase in antibacterial activity observed in NPs with large surface areas[86].

Previous studies have highlighted the critical role of AuNPs in drug delivery, showcasing their capacity to tackle a wide array of pathogenic bacteria through potent antibacterial effects[87–89]. Consequently, AuNPs synthesized using *A. compressa* extract emerge as promising candidates for antibacterial drugs, holding potential for both current and future applications in combating bacterial infections. Supporting this, Muniyappan et al.[90] proved that CUR-AuNPs possess significant antibacterial activity. At a concentration of 300 µg/mL, CUR-AuNPs showed the largest area of inhibition against *E. coli, B. subtilis, S. aureus*, and *P. aeruginosa* were 28, 26, 25, and 23 mm, respectively. Using the agar well diffusion method, Nagalingam et al.[91] reported that AuNPs made from *A. bettzickiana* leaf extract had good antibacterial qualities against a range of bacterial species, such as *B. subtilis, S. aureus, S. typhi, P. aeruginosa, M. luteus*, and *E. aerogenes*.

The size and morphology of nanoparticles play a crucial role in determining their antimicrobial efficacy[92]. In the present study, TEM and SEM analyses revealed that the biosynthesized AuNPs were small, spherical, and well-dispersed. These nanoscale dimensions are associated with a high surface area-to-volume ratio, which enhances the interaction between the nanoparticles and microbial cell membranes. As smaller particles can penetrate bacterial cell walls more easily, they tend to disrupt membrane integrity, generate reactive oxygen species (ROS), and interfere with intracellular components more effectively[93]. These mechanisms collectively contribute to the strong antimicrobial activity observed in the synthesized AuNPs[94]. Our findings are consistent with previous reports indicating that nanoparticles with smaller sizes generally exhibit superior antimicrobial properties[95,96].

Biofilm formation arises from the aggregation of free-living planktonic bacteria, driven by physiological processes such as motility, surface attachment, proliferation, differentiation, and the development of multilayered cellular structures within an extracellular polymeric matrix[97]. Numerous studies have shown that this matrix serves as a protective barrier, shielding the cells from antibiotics, detergents, disinfectants, and host immune responses, thereby contributing to their resistance. Consequently, controlling biofilm formation is crucial[98–100]. The efficacy of green-synthesized AuNPs in biofilm inhibition was assessed through colorimetric assays against various pathogenic bacterial strains, with the results presented in Figs. 7. These findings indicated that AuNPs exhibited the most significant biofilm inhibition activity against all tested bacterial strains.

Supporting these results, Khan et al.[101], utilizing AuNPs synthesized from *Clerodendrum inerme* for antimicrobial and antibiofilm activities, corroborates these results. Likewise, Perveen et al.[17] highlighted the effectiveness of TA-AuNPs in preventing biofilm formation by *S. marcescens* and *Listeria monocytogenes*, further underscoring the potential of AuNPs in biofilm control. Interestingly, Arief et al.[102], it was found that AuNPs actually stimulated the formation of biofilms but also interacted with components of the cell wall, resulting in structural alterations, degradation, and ultimately cell death. During this interaction, the AuNPs became entrapped within the biofilm and released certain compounds, which induced distortions in the cell wall. This dual action of AuNPs underscores their complex interaction with bacterial cells and biofilms, highlighting both their potential to influence biofilm formation and their antimicrobial efficacy through the disruption of cell wall integrity.

To further elucidate the anti-inflammatory mechanism, the membrane stabilization of RBCs was assessed. This investigation offered evidence that membrane stabilization contributes to the anti-inflammatory effects observed. It is proposed that both *A. compressa* extract and AuNPs could inhibit the release of lysosomal contents from neutrophils at inflammation sites. These lysosomal constituents, which include proteases and bactericidal enzymes, might worsen tissue injury and inflammation when they are discharged extracellularly[90,103]. This understanding provides further insight into how *A. compressa* extract and AuNPs may offer therapeutic benefits in controlling inflammation.

Metallic nanoparticles have been recognized for their significant role in neutralizing harmful free radicals such as DPPH[104]. In this context, DPPH radicals (DPPH•) are reduced to their non-radical form (DPPH-H) upon accepting hydrogen or electrons from antioxidant agents like AuNPs and *A. compressa* extract. This research aimed to track the reduction in DPPH levels resulting from its interaction with both AuNPs and *A. compressa* extract, using a spectrophotometer for measurement. The findings, illustrated in Table 2, demonstrated that all tested antioxidant samples inhibited the DPPH free radical in a manner dependent on their concentration. Moreover, AuNPs, particularly those synthesized through eco-friendly methods, showed a marked ability to prevent oxidative damage[53]. Hosny et al.[105], reported that the antioxidant effectiveness of *T. capensis*-AuNPs is influenced by the phytochemicals in *T. capensis*, such as alkaloids that encase the nanoparticles, as the *T. capensis* water extract itself showed significant antioxidant activity.

Supporting these findings, several studies have observed stronger antioxidant activity in aqueous plant extracts compared to the AuNPs synthesized from them. For instance, Zayed et al.[106] reported that the extract of *Pimpinella anisum* was a more potent antioxidant than its AuNP counterpart, and Sathishkumar et al.[107], found that *Couroupita guianensis* extract had greater inhibitory power compared to AuNPs synthesized from it. Similarly, Nakkala et al.[108] noted that the *Costus pictus* extract exhibited higher antioxidant effectiveness than the AuNPs derived from the same extract. These outcomes are thought to stem from the potent reducing abilities of the plant extracts, leading to their elevated antioxidant efficacy[109,110]. In a study conducted by Al-Radadi,[111], the antioxidant capacities were assessed using DPPH and ABTS methods. The IC50 values, which indicate the concentration required to inhibit 50% of the free radicals, for licorice root extract, DPPH, and AuNPs were found to be 86.90, 78.89, and 74.50 mg/mL, respectively. Similarly, when evaluated with the ABTS method, the IC50 values for licorice root extract, ABTS, and AuNPs were 83.81, 79.00, and 77.65 mg/mL, respectively. It was noted that flavonoids and phenolic compounds in the extracts are primarily responsible for their antioxidant effects, functioning through the donation of electrons to neutralize free radicals. Chen et al.[79] highlighted that gold nanoparticles, synthesized through eco-friendly methods, possess impressive redox capabilities, playing a crucial role in neutralizing free radicals. Furthermore cancer by Zahra et al.[112], has underscored the importance

of antioxidant agents in treating various types of cancer, including blood, colon, ovarian, lung, and pancreatic cancers.

In developing countries, vector-borne diseases transmitted by flies and mosquitoes remain a major public health concern. The continued reliance on synthetic insecticides has become increasingly problematic due to the development of insect resistance and the associated toxicity risks to humans and non-target organisms. These challenges have spurred growing interest in exploring more environmentally sustainable alternatives[113]. Marine sponge extracts have shown promising insecticidal potential[25], and recent evidence suggests that nanoparticles synthesized using eco-friendly methods may offer superior efficacy compared to crude extracts alone[114]. Despite this, limited research has been conducted on the toxicity of nanoparticles against *M. demostica* and *C. pipiens*[26,51,115]. In our study, both the crude extract and biosynthesized AuNPs exhibited potent adulticidal activity. For *M. domestica*, the LC50 and LC90 values were 34.988 and 62.836 µL/adult for the crude extract, and 8.545 and 15.157 µL/adult for the AuNPs, respectively. Mortality reached 93.33% at 60 µL/adult with the crude extract, while complete mortality (100%) was observed at just 20 µL/adult with AuNPs. Similarly, in C. pipiens, LC50 and LC90 values were 9.258 and 17.399 ppm for the crude extract, and 7.573 and 14.074 ppm for the AuNPs, respectively. The crude extract caused 96.67% mortality at 20 ppm, whereas the AuNPs achieved 100% mortality at only 16 ppm. Our findings are in line with those of Soni and Prakash[116], who found that after four hours of exposure, adulticidal activity of *C. quinquefasciatus* was increased by AgNPs generated from *Azadirachta indica*, with an LC50 of 1.06 µL/cm^2. Likewise, Veerakumar and Govindarajan[117] demonstrated that Feronia elephantum-derived AgNPs were toxic to adult stages of *Anopheles stephensi*, *Aedes aegypti*, and *Culex quinquefasciatus*, with LD50values of 18.04, 20.39, and 21.798 µg/mL, respectively. Benelli et al.[118] reported that *Acacia caesia* leaf extract and biosynthesized AgNPs have a high adulticidal action against *A. Subpictus* (LD50 = 18.66 µg/ml), *A. Albopictus* (LD50 = 20.94 µg/ml), and *C. tritaeniorhynchus* (LD50 = 22.63 µg/ml). Our results are similar to their findings. Additionally, the findings of Suresh et al.[119] showed that adulticidal behavior had LC50 and LC90 values of 174.14 and 422.29 for the crude, and 6.68 ppm and 23.58 ppm for *Phyllanthus niruri* AgNPs respectively, end with mortality of treated adults.

The fecundity and hatchability of both *M. domestica* and *C. pipiens* mosquitoes decreased significantly with increasing concentrations of both crude and biosynthesized AuNPs extracts. For *M. domestica*, the lowest recorded fecundity and hatchability occurred at concentrations of 60 µL/adult for the crude extract and 12 µL/adult for the AuNPs. Similarly, in *C. pipiens*, the minimum values were observed at 20 ppm and 16 ppm for the crude and AuNPs extracts, respectively. The reductions were markedly more pronounced in the groups treated with AuNPs compared to those treated with the crude extract. Compared to the crude extract, the benefits were significantly more noticeable in the AuNPs extract. The crude extract of *S. officinalis* and So-ZnO-NPs administered at different doses had an unfavourable relationship with fecundity[25]. At a concentration of 80 ppm of So-ZnO-NPs, the fecundity of *C. pipiens* females was dramatically reduced to more than 50%, and this impact was even more severe in female *A. pharoensis* at concentrations over 40 ppm when compared to the untreated control[26]. According to Roni et al.[120], the female fecundity of *A. Aegypti* was significantly decreased by concentrations of *Hypnea musciformis*-fabricated AgNP ranging from 100 to 500 ppm. In addition, Madhiyazhagan et al.[121] found that *S. Muticum*-generated AgNP reduced oviposition rates to over 70% in *A. aegypti*, *A. stephensi*, and *C. quinquefasciatus* when administered at a concentration of 10 ppm. While control eggs showed 100% hatchability in the same environment, A. aegypti, *A. stephensi*, and *C. quinquefasciatus* eggs showed 100% hatchability after treatment with 30 ppm of AgNP[121]. Furthermore, Barik et al.[122] investigated the behavior of three distinct mosquito species amid different types of nanosilica during oviposition. While lipophilic nanosilica had no influence on the oviposition behavior of the three vectors, hydrophobic nanosilica demonstrated 100% ovideterrence activity against *A. aegypti*, *A. stephensi*, and *C. quinquefasciatus* at 112.5 ppm.

Conclusion

Using a green chemistry approach, we successfully synthesized (AuNPs using *A. compressa* extract. The biosynthesized AuNPs, measuring 10–40 nm with predominantly spherical to oval morphology, were produced without the use of harmful chemicals or pH adjustments, emphasizing the eco-friendly and scalable nature of the synthesis method. The particle size range was confirmed by TEM analysis and further supported by XRD-based crystallite size estimation, which yielded an average size of 29.21 nm validating the nanoscale dimensions and crystalline structure of the synthesized particles. This approach also ensured high nanoparticle stability in solution. The AuNPs showed strong antimicrobial activity against four pathogenic bacteria (inhibition zones: 26–31 mm), alongside significant antioxidant (70.73%) and anti-inflammatory effects (hemolysis inhibition: 4.8%–22.4%). Furthermore, the biosynthesized AuNPs exhibited effective larvicidal and adulticidal activity against *M. domestica* and *C. pipiens*, with *C. pipiens* being more sensitive to the nanoparticles than the crude extract. These findings demonstrate the potential of marine sponge-based AuNPs as sustainable, effective agents in biomedical and vector control applications.

Data availability

Supplementary information files have been included as part of the manuscript submission.In addition, the primary datasets supporting the findings of this study (e.g., XRD and FTIR data) have been deposited in the Figshare repository and are publicly available via the following https://doi.org/10.6084/m9.figshare.29390426.

Received: 7 February 2025; Accepted: 14 July 2025
Published online: 30 July 2025

References

1. Zahin, N. et al. Research, P. Nanoparticles and its biomedical applications in health and diseases: special focus on drug delivery. *Environ. Sci. Pollution Res.* **27**, 19151–19168 (2020).
2. Nikolaidis, P.J.G.s.o.n.f.b.a. Analysis of green methods to synthesize nanomaterials. Green synthesis of nanomaterials for bioenergy applications,125–144. (**2020).**
3. Kumar, J. A. et al. A focus to green synthesis of metal/metal based oxide nanoparticles: Various mechanisms and applications towards ecological approach. *J. Clean. Prod.* **324**, 129198 (2021).
4. Dikshit, P. K. et al. Green synthesis of metallic nanoparticles: Applications and limitations. *Catalysts* **11**, 902 (2021).
5. Huston, M., DeBella, M., DiBella, M. & Gupta, A. J. N. Green synthesis of nanomaterials. *Nanomaterials* **11**, 2130 (2021).
6. Bansal, S. A., Kumar, V., Karimi, J., Singh, A. P. & Kumar, S. J. N. A. Role of gold nanoparticles in advanced biomedical applications. *Nanoscale Advances* **2**, 3764–3787 (2020).
7. Chinemerem Nwobodo, D. et al. Antibiotic resistance: The challenges and some emerging strategies for tackling a global menace. *J. Clin. Lab Anal.* **36**, e24655 (2022).
8. Varela, M. F. et al. Bacterial resistance to antimicrobial agents. *Antibiotics* **10**, 593 (2021).
9. Dey, N. et al. Role of nanomaterials in deactivating multiple drug resistance efflux pumps–A review. *Environ. Res.* **204**, 111968 (2022).
10. Hessling, M., Feiertag, J. & Hoenes, K. J. B. B. R. C. Pathogens provoking most deaths worldwide. *Res. Commun.* **10**, 1–7 (2017).
11. Jansen, K. U., Gruber, W. C., Simon, R., Wassil, J. & Anderson, A. S. J. E. C. L. The impact of human vaccines on bacterial antimicrobial resistance. *A Rev. Environ. Chem. letters.* **19**, 4031–4062 (2021).
12. Fatima, F., Siddiqui, S. & Khan, W. A. J. B. T. E. R. Nanoparticles as novel emerging therapeutic antibacterial agents in the antibiotics resistant era. *Biol. Trace Element Res.* **199**, 2552–2564 (2021).
13. Bhattacharjee B, Ghosh S, Patra D, Haldar J J W I R N. Nanobiotechnology. Advancements in release-active antimicrobial biomaterials: A journey from release to relief. Wiley Interdisciplinary Reviews: Nanomedicine and Nanobiotechnology. *14*, e1745. (**2022).**
14. Muhammad, M. H., Idris, A. L. & Huang, T. J. F. I. M. Beyond risk: bacterial biofilms and their regulating approaches. *Front. Microbiol.* **11**, 530515 (2020).
15. Priyadarshanee, M. & Das, S. J. C. Bacterial extracellular polymeric substances: biosynthesis and interaction with environmental pollutants. *Chemosphere* **332**, 138876 (2023).
16. Hrynyshyn, A., Simões, M. & Borges, A. J. A. Biofilms in surgical site infections: recent advances and novel prevention and eradication strategies. *Antibiotics* **11**, 69 (2022).
17. Perveen, K. et al. Microwave-assisted rapid green synthesis of gold nanoparticles using seed extract of Trachyspermum ammi: ROS mediated biofilm inhibition and anticancer activity. *Biomolecules* **11**, 197 (2021).
18. Garofalo, C. et al. Current knowledge on the microbiota of edible insects intended for human consumption: A state-of-the-art review. *Food Res. Int.* **125**, 108527 (2019).
19. Di Meo, S.; Venditti, P.J.O.m.; longevity, c. Evolution of the knowledge of free radicals and other oxidants. **2020**, *2020*.
20. Martemucci, G. et al. Free radical properties, source and targets, antioxidant consumption and health. *Oxygen* **2**, 48–78 (2022).
21. Davies, M. P., Anderson, M. & Hilton, A. C. The housefly Musca domestica as a mechanical vector of Clostridium difficile. *J. Hosp. Infect.* **94**, 263–267. https://doi.org/10.1016/j.jhin.2016.08.023 (2016).
22. Cromwell, E. A. et al. The global distribution of lymphatic filariasis, 2000–18: a geospatial analysis. *Lancet Glob. Health* **8**, e1186–e1194 (2020).
23. Ghosh, A., Chowdhury, N. & Chandra, G. J. I. J. O. M. R. Plant extracts as potential mosquito larvicides. *Indian J. Med. Res.* **135**, 581–598 (2012).
24. Prasad, A. R. et al. Applications of phytogenic ZnO nanoparticles: A review on recent advancements. *J. Mol. Liq.* **331**, 115805. https://doi.org/10.1016/j.molliq.2021.115805 (2021).
25. Hasaballah, A. I., El-Naggar, H. A., Abdelbary, S., Bashar, M. A. E. & Selim, T. A. Eco-friendly Synthesis of Zinc Oxide Nanoparticles by Marine Sponge, Spongia officinalis: Antimicrobial and Insecticidal Activities Against the Mosquito Vectors. *Culex pipiens and Anopheles pharoensis. BioNanoSci.* **12**, 89–104. https://doi.org/10.1007/s12668-021-00926-2 (2022).
26. Hasaballah, A., Selim, T., Tanani, M. & Nasr, E. J. A. E. Lethality and vitality efficiency of different extracts of Salix safsaf leaves against the house fly, Musca domestica L. (Diptera: Muscidae). *African Entomol.* **29**, 479–490 (2021).
27. Mehlhorn, H. Nanoparticles – Definitions. In *Nanoparticles in the Fight Against Parasites* (ed. Mehlhorn, H.) 1–14 (Springer International Publishing, 2016).
28. Patra, J. K. et al. Nano based drug delivery systems: recent developments and future prospects. *Journal of Nanobiotechnology.* **16**, 71. https://doi.org/10.1186/s12951-018-0392-8 (2018).
29. Adamska, M. *Phylum Porifera* 121–136 (CRC Press, 2021).
30. Fromont J J B R O T M. Art Galleries of the Northern Territory T. Descriptions of species of the Haplosclerida (Porifera: Demospongiae) occurring in tropical waters of the Great Barrier Reef. Beagle: Records of the Museums and Art Galleries of the Northern Territory. *10*, 7–40. (**1993)**
31. Waddell, B. & Pawlik, J. R. J. M. E. P. S. Defenses of Caribbean sponges against invertebrate predators. II. Assays with sea stars. *Mar. Ecol. Prog. Ser.* **195**, 133–144 (2000).
32. Hussni Hasan, N. R. et al. From the Sea to Mosquito Control: The Potential of Halymenia dilatata Marine Alga as an Eco-Friendly Mosquitocidal Agent. *Sustainability* **15**, 11900 (2023).
33. Mansour, S.A.; Bakr, R.F.; Hamouda, L.S.; Mohamed, R.I.J.E.A.J.o.B.S.A., Entomology. Adulticidal activity of some botanical extracts, commercial insecticides and their binary mixtures against the housefly, Musca domestica L. Egyptian Academic Journal of Biological Sciences. A, Entomology, **2012**, *5*, 151–167.
34. Hooper, J.N.; Van Soest, R.W. Systema Porifera. A guide to the classification of sponges. In *Systema Porifera: A guide to the classification of sponges*; Springer: 2002; pp. 1–7.
35. Nele, A. N, Hooper JNA, Rützler K, de Voogd NJ, Alvarez de Glasby B, Hajdu E, Pisera AB, Manconi R, Schönberg CHL, Janussen D, Tabachnick KR, Klautau M, Picton B, Kelly M, Vacelet J, Dohrmann M, Díaz M--C, Cárdenas P World Porifera Database. Accessed at http://www. marinespecies. org/porifera on.https://www.researchgate.net/publication/278616972 (2015)
36. Abdel-Raouf, N., Al-Enazi, N. M. & Ibraheem, I. B. J. A. J. O. C. Green biosynthesis of gold nanoparticles using Galaxaura elongata and characterization of their antibacterial activity. *Arabian J. Chem.* **10**, S3029–S3039 (2017).
37. Valsalam, S. et al. Biosynthesis of silver and gold nanoparticles using Musa acuminata colla flower and its pharmaceutical activity against bacteria and anticancer efficacy. *J. Photochem. Photobiol., B* **201**, 111670. https://doi.org/10.1016/j.jphotobiol.2019.111670 (2019).
38. Abdel-Maksoud, G.; Abdel-Nasser, M.; Hassan, S.E.-D.; Eid, A.M.; Abdel-Nasser, A.; Fouda, A.J.B.C.; Biorefinery. Biosynthesis of titanium dioxide nanoparticles using probiotic bacterial strain, Lactobacillus rhamnosus, and evaluate of their biocompatibility and antifungal activity. Biomass Conversion and Biorefinery, 1–23. (**2023).**
39. Ganesan, V., Hariram, M., Vivekanandhan, S. & Muthuramkumar, S. J. M. S. I. S. P. Periconium sp (endophytic fungi) extract mediated sol-gel synthesis of ZnO nanoparticles for antimicrobial and antioxidant applications. *Mater. Sci. Semiconductor Proc.* **105**, 104739 (2020).
40. Saied, E. et al. Mycosynthesis of hematite (α-Fe2O3) nanoparticles using Aspergillus niger and their antimicrobial and photocatalytic activities. *Bioengineering* **9**, 397 (2022).

41. Shehabeldine, A. M. et al. Multifunctional silver nanoparticles based on chitosan: Antibacterial, antibiofilm, antifungal, antioxidant, and wound-healing activities. *J. Fungi.* **8**, 612 (2022).
42. Rodríguez-Melcón, C., Alonso-Calleja, C., García-Fernández, C., Carballo, J. & Capita, R. J. B. Minimum inhibitory concentration (MIC) and minimum bactericidal concentration (MBC) for twelve antimicrobials (biocides and antibiotics) in eight strains of Listeria monocytogenes. *Biology* **11**, 46 (2021).
43. Luna-Vázquez-Gómez, R. et al. Hemolysis of human erythrocytes by Argovit™ AgNPs from healthy and diabetic donors: An in vitro study. *Materials* **14**, 2792 (2021).
44. Mekky, A. E. et al. Unravelling the Antimicrobial, Antibiofilm, Suppressing Fibronectin Binding Protein A (fnba) and cna Virulence Genes, Anti-Inflammatory and Antioxidant Potential of Biosynthesized Solanum lycopersicum Silver Nanoparticles. *Medicina* **60**, 515 (2024).
45. Soliman, M. K., Salem, S. S., Abu-Elghait, M. & Azab, M. S. J. A. B. Biotechnology. Biosynthesis of silver and gold nanoparticles and their efficacy towards antibacterial, antibiofilm, cytotoxicity, and antioxidant activities. *Appl. Biochem. Biotechnol.* **195**, 1158–1183 (2023).
46. Ertas Onmaz, N. et al. Green synthesis of gold nanoflowers using Rosmarinus officinalis and Helichrysum italicum extracts: Comparative studies of their antimicrobial and antibiofilm activities. *Antibiotics.* **11**, 1466 (2022).
47. Mtaki, K., Kyewalyanga, M. S. & Mtolera, M. S. J. A. S. Assessment of antioxidant contents and free radical-scavenging capacity of chlorella vulgaris cultivated in low cost media. *Appl. Sci.* **10**, 8611 (2020).
48. Loucif, K. et al. Therapeutics. Total phenolic contents, DPPH radical scavenging and β-carotene bleaching activities of aqueous extract from Ammoides atlantica. *J. Drug Delivery Therapeutics.* **10**, 196–198 (2020).
49. Mansour S, Bakr R, Mohamed R, Hasaneen N J S. Larvicidal activity of some botanical extracts, commercial insecticides and their binary mixtures against the housefly, MuscaDomestica L. Egyptian Academic Journal of Biological Sciences. A, Entomology, *10*, 100.100. (**2011**)
50. Organization, W.H. Instructions for determining the susceptibility or resistance of adult mosquitoes to organochlorine, organophosphorus and carbamate insecticides: establishment of the base-line. In *Instructions for determining the susceptibility or resistance of adult mosquitoes to organochlorine, organophosphorus and carbamate insecticides: establishment of the base-line*; (1981).
51. Hasaballah, A. I. Impact of paternal transmission of gamma radiation on reproduction, oogenesis, and spermatogenesis of the housefly, Musca domestica L. (Diptera: Muscidae). *Int. J. Radiation Biol.* **97**, 376–385. https://doi.org/10.1080/09553002.2021.1864046 (2021).
52. Rak, S. & Ishii, T. J. J. S. U. T. Characters eggs and egg masses obtained by induced oviposition in Culex pipiens L. *J. Sci. Univ. Tokushima.* **22**, 25–31 (1989).
53. Santhosh, P. B., Genova, J. & Chamati, H. J. C. Green synthesis of gold nanoparticles: An eco-friendly approach. *Chemistry* **4**, 345–369 (2022).
54. Kim, B., Song, W. C., Park, S. Y. & Park, G. J. C. Green synthesis of silver and gold nanoparticles via Sargassum serratifolium extract for catalytic reduction of organic dyes. *Catalysts* **11**, 347 (2021).
55. Donga, S., Bhadu, G. R. & Chanda, S. J. A. C. Nanomedicine Biotechnology. Antimicrobial, antioxidant and anticancer activities of gold nanoparticles green synthesized using Mangifera indica seed aqueous extract. *Artificial cells, Nanomedicine, Biotechnol.* **48**, 1315–1325 (2020).
56. Zayadi, R. A. & Bakar, F. A. J. J. O. E. C. E. Comparative study on stability, antioxidant and catalytic activities of bio-stabilized colloidal gold nanoparticles using microalgae and cyanobacteria. *J. Environ. Chem. Eng.* **8**, 103843 (2020).
57. Amina, S. J. et al. Synthesis of diosgenin conjugated gold nanoparticles using algal extract of Dictyosphaerium sp and in-vitro application of their antiproliferative activities. *Materials Today Communications.* **27**, 102360 (2021).
58. Mariychuk, R. et al. The regularities of the Mentha piperita L. extract mediated synthesis of gold nanoparticles with a response in the infrared range. *Appl. Nanosci.* **12**, 1071–1083 (2022).
59. Kamaraj, C. et al. Green synthesis of gold nanoparticles using Gracilaria crassa leaf extract and their ecotoxicological potential: Issues to be considered. *Environ. Res.* **213**, 113711 (2022).
60. Shah, S. et al. Engineering novel gold nanoparticles using Sageretia thea leaf extract and evaluation of their biological activities. *J. Nanostructure Chem.* **12**, 129–140 (2022).
61. Borse, V. & Konwar, A. N. J. S. I. Synthesis and characterization of gold nanoparticles as a sensing tool for the lateral flow immunoassay development. *Sensors Int.* **1**, 100051 (2020).
62. Clarance, P. et al. Green synthesis and characterization of gold nanoparticles using endophytic fungi Fusarium solani and its in-vitro anticancer and biomedical applications. *Saudi J. Biol. Sci.* **27**, 706–712 (2020).
63. Pitchai, P. et al. Green synthesis of gold nanoparticles (AuNPs) using Caulerpa racemosa and evaluation of its antibacterial and cytotoxic activity against human lung cancer cell line. *Arab J. Basic Appl. Sci.* **29**, 351–362 (2022).
64. Paramasivam, V. et al. Cytotoxicity and Antimicrobial efficiency of gold (Au) nanoparticles formulated by green approach using Andrographis paniculata leaf extract. *J. King Saud Univ.-Sci.* **35**, 102687 (2023).
65. Rokkarukala, S.; Cherian, T.; Ragavendran, C.; Mohanraju, R.; Kamaraj, C.; Almoshari, Y.; Albariqi, A.; Sultan, M.H.; Alsalhi, A.; Mohan, S.J.H. One-pot green synthesis of gold nanoparticles using Sarcophyton crassocaule, a marine soft coral: assessing biological potentialities of antibacterial, antioxidant, anti-diabetic and catalytic degradation of toxic organic pollutants. Heliyon. *9*. **(2023)**
66. Sarfraz, N. & Khan, I. J. C. A. A. J. Plasmonic gold nanoparticles (AuNPs): properties, synthesis and their advanced energy environmental and biomedical applications. *Chem.-An Asian J.* **16**, 720–742 (2021).
67. Philip, A. & Kumar, A. R. J. C. C. R. The performance enhancement of surface plasmon resonance optical sensors using nanomaterials: A review. *Coord. Chem. Rev.* **458**, 214424 (2022).
68. Wongyai, K., Wintachai, P., Maungchang, R. & Rattanakit, P. J. J. O. N. Exploration of the antimicrobial and catalytic properties of gold nanoparticles greenly synthesized by Cryptolepis buchanani Roem. and Schult extract. *J. Nanomater.* **2020**, 1–11 (2020).
69. El-Sheekh, M. M., Hassan, L. H. & Morsi, H. H. J. R. L. S. F. E. N. Evaluation of antimicrobial activities of blue-green algae-mediated silver and gold nanoparticles. *Rendiconti Lincei. Sci. Fisiche e Nat.* **32**, 747–759 (2021).
70. Ahmad, T., Iqbal, J., Bustam, M. A., Irfan, M. & Asghar, H. M. A. J. J. O. C. P. A critical review on phytosynthesis of gold nanoparticles: Issues, challenges and future perspectives. *J. Clean. Prod.* **309**, 127460 (2021).
71. Sidhu, A. K., Verma, N. & Kaushal, P. J. F. I. N. Role of biogenic capping agents in the synthesis of metallic nanoparticles and evaluation of their therapeutic potential. *Front. Nanotechnol.* **3**, 801620 (2022).
72. Batsale, M. et al. Biosynthesis and functions of very-long-chain fatty acids in the responses of plants to abiotic and biotic stresses. *Cells* **10**, 1284 (2021).
73. Oliveira, J.M.; Radhouani, H.; Reis, R.L. *Polysaccharides of Microbial Origin*; Springer: (2022).
74. Shera, S. S. & Banik, R. M. *Algal nanoparticles: synthesis and characterization* 25–69 (Springer, 2022).
75. Sathiyaraj, S. et al. Health, P. Biosynthesis, characterization, and antibacterial activity of gold nanoparticles. *J. Inf. Public Health* **14**, 1842–1847 (2021).
76. Folorunso, A. et al. Biosynthesis, characterization and antimicrobial activity of gold nanoparticles from leaf extracts of Annona muricata. *J. Nanostructure Chem.* **9**, 111–117 (2019).
77. Babu, B. et al. engineering, b. Bioengineered gold nanoparticles from marine seaweed Acanthophora spicifera for pharmaceutical uses: antioxidant, antibacterial, and anticancer activities. *Bioprocess Biosyst. Eng.* **43**, 2231–2242 (2020).

78. Subbulakshmi, A. et al. Biogenic gold nanoparticles from Gelidiella acerosa: bactericidal and photocatalytic degradation of two commercial dyes. *Appl. Nanosci.* **13**, 4033–4042 (2023).
79. Chen, J. et al. Green synthesis, characterization, cytotoxicity, antioxidant, and anti-human ovarian cancer activities of Curcumae kwangsiensis leaf aqueous extract green-synthesized gold nanoparticles. *Arab. J. Chem.* **14**, 103000 (2021).
80. Paesa, M. et al. Science, I. Elucidating the mechanisms of action of antibiotic-like ionic gold and biogenic gold nanoparticles against bacteria. *J. Colloid Interface Sci.* **633**, 786–799 (2023).
81. Motevaseli E, Dianatpour A, Ghafouri-Fard S J I J O M. Medicine, c. The role of probiotics in cancer treatment: emphasis on their in vivo and in vitro anti-metastatic effects. International journal of molecular and cellular medicine, *6*, 66. **(2017).**
82. Hamad, A., Khashan, K. S., Hadi, A. J. J. & o I, Polymers O.,. Materials. Silver nanoparticles and silver ions as potential antibacterial agents. *J. Inorg. Organomet. Polym Mater.* **30**, 4811–4828 (2020).
83. Kaushal, P.; Maity, D.; Awasthi, R.J.J.o.D.D.S.; Technology. Nano-green: Harnessing the potential of plant extracts for sustainable antimicrobial metallic nanoparticles. Journal of Drug Delivery Science and Technology, **2024**, 105488.
84. Abdalla, S. S., KatasH Azmi, F. & Busra, M. F. M. J. C. D. D. Antibacterial and anti-biofilm biosynthesised silver and gold nanoparticles for medical applications: Mechanism of action, toxicity and current status. *Curr. Drug Deliv.* **17**, 88–100 (2020).
85. Mohamed, D. S., Abd El-Baky, R. M., Sandle, T., Mandour, S. A. & Ahmed, E. F. J. A. Antimicrobial activity of silver-treated bacteria against other multi-drug resistant pathogens in their environment. *Antibiotics* **9**, 181 (2020).
86. Taye, M. B., Ningsih, H. S. & Shih, S. J. J. J. O. N. R. Exploring the advancements in surface-modified bioactive glass: enhancing antibacterial activity, promoting angiogenesis, and modulating bioactivity. *J. Nanoparticle Res.* **26**, 28 (2024).
87. Song, M. et al. Research Progress of Polysaccharide-Gold Nanocomplexes in Drug Delivery. *Pharmaceutics* **16**, 88 (2024).
88. Devi, L.; Kushwaha, P.; Ansari, T.M.; Kumar, A.; Rao, A.J.B.T.E.R. Recent trends in biologically synthesized metal nanoparticles and their biomedical applications: a review. Biological Trace Element Research, **2023**, 1–17.
89. Fadaka, A. O., Sibuyi, N. R. S., Madiehe, A. M. & Meyer, M. J. P. Nanotechnology-based delivery systems for antimicrobial peptides. *Pharmaceutics* **13**, 1795 (2021).
90. Muniyappan, N., Pandeeswaran, M. & Amalraj, A. J. E. C. Ecotoxicology. Green synthesis of gold nanoparticles using Curcuma pseudomontana isolated curcumin: Its characterization, antimicrobial, antioxidant and anti-inflammatory activities. *Environ. Chem. Ecotoxicol.* **3**, 117–124 (2021).
91. Nagalingam, M., Kalpana, V. N. & Panneerselvam, A. J. B. R. Biosynthesis, characterization, and evaluation of bioactivities of leaf extract-mediated biocompatible gold nanoparticles from Alternanthera bettzickiana. *Biotechnol. Rep.* **19**, e00268 (2018).
92. Sayed, F.A.-Z. et al. Morphologic design of nanostructures for enhanced antimicrobial activity. *J. Nanobiotechnol.* **20**, 536. https://doi.org/10.1186/s12951-022-01733-x (2022).
93. Zhang, J. et al. Impact of reactive oxygen species on cell activity and structural integrity of Gram-positive and Gram-negative bacteria in electrochemical disinfection system. *Chem. Eng. J.* **451**, 138879. https://doi.org/10.1016/j.cej.2022.138879 (2023).
94. He, J. et al. Progress and prospects of nanomaterials against resistant bacteria. *J. Control. Release* **351**, 301–323. https://doi.org/10.1016/j.jconrel.2022.09.030 (2022).
95. Fan, X., Yahia, L. H. & Sacher, E. Antimicrobial Properties of the Ag. *Cu Nanoparticle Syst.* **10**, 137 (2021).
96. Piktel, E. et al. Varied-shaped gold nanoparticles with nanogram killing efficiency as potential antimicrobial surface coatings for the medical devices. *Sci. Rep.* **11**, 12546. https://doi.org/10.1038/s41598-021-91847-3 (2021).
97. Alotaibi, G. F. & Bukhari, M. A. J. A. J. B. S. R. Factors influencing bacterial biofilm formation and development. *Am. J. Biomed. Sci. Res* **12**, 617–626 (2021).
98. Singh, A. et al. Bacterial biofilm infections, their resistance to antibiotics therapy and current treatment strategies. *Biomed. Mater.* **17**, 022003 (2022).
99. Singh, S., Datta, S., Narayanan, K. B. & Rajnish, K. N. J. J. O. G. E. Bacterial exo-polysaccharides in biofilms: role in antimicrobial resistance and treatments. *J. Gene. Eng. Biotechnol.* **19**, 1–19 (2021).
100. Dincer, S.; Uslu, F.M.; Delik, A. Antibiotic resistance in biofilm. In *Bacterial biofilms*; IntechOpen: 2020.
101. Khan, S. A., Shahid, S. & Lee, C.-S.J.B. Green synthesis of gold and silver nanoparticles using leaf extract of Clerodendrum inerme; characterization, antimicrobial, and antioxidant activities. *Biomolecules* **10**, 835 (2020).
102. Arief, S., Nasution, F. W. & Labanni, A. J. J. O. A. P. S. High antibacterial properties of green synthesized gold nanoparticles using Uncaria gambir Roxb. leaf extract and triethanolamine. *Journal of Applied Pharmaceutical Science* **10**, 124–130 (2020).
103. Yesmin S, PaulA Naz T, Rahman A A, Akhter S F, Wahed M I I, Emran T B, Siddiqui S A J C P. **2020** Membrane stabilization as a mechanism of the anti-inflammatory activity of ethanolic root extract of Choi (Piper chaba) Clinical Phytoscience, *6*, 1–10.
104. Kumar, H. et al. Antioxidant functionalized nanoparticles: A combat against oxidative stress. *Nanomaterials* **10**, 1334 (2020).
105. Hosny, M., Fawzy, M., El-Badry, Y. A., Hussein, E. E. & Eltaweil, A. S. J. J. O. S. C. S. Plant-assisted synthesis of gold nanoparticles for photocatalytic, anticancer, and antioxidant applications. *J. Saudi Chem. Soc.* **26**, 101419 (2022).
106. Zayed, M. F. et al. In-vitro antioxidant and antimicrobial activities of metal nanoparticles biosynthesized using optimized Pimpinella anisum extract. *Colloids Surf., A* **585**, 124167 (2020).
107. Sathishkumar, G. et al. Cannonball fruit (Couroupita guianensis, Aubl.) extract mediated synthesis of gold nanoparticles and evaluation of its antioxidant activity. *J. Mol. Liquids.* **215**, 229–236 (2016).
108. Nakkala, J. R., Bhagat, E., Suchiang, K. & Sadras, S. R. J. J. O. M. S. Technology. Comparative study of antioxidant and catalytic activity of silver and gold nanoparticles synthesized from Costus pictus leaf extract. *J. Mater. Sci. Technol.* **31**, 986–994 (2015).
109. Eltaweil, A. S. et al. Green synthesis of platinum nanoparticles using Atriplex halimus leaves for potential antimicrobial, antioxidant, and catalytic applications. *Arabian J. Chem.* **15**, 103517 (2022).
110. Pateiro, M., Gómez-Salazar, J. A., Jaime-Patlán, M., Sosa-Morales, M. E. & Lorenzo, J. M. J. A. Plant extracts obtained with green solvents as natural antioxidants in fresh meat products. *Antioxidants* **10**, 181 (2021).
111. Al-Radadi, N. S. J. A. J. O. C. Facile one-step green synthesis of gold nanoparticles (AuNp) using licorice root extract: Antimicrobial and anticancer study against HepG2 cell line. *Arabian J. Chem.* **14**, 102956 (2021).
112. Zahra, K.F.; Lefter, R.; Ali, A.; Abdellah, E.-C.; Trus, C.; Ciobica, A.; Timofte, D.J.O.M.; Longevity, C. The involvement of the oxidative stress status in cancer pathology: A double view on the role of the antioxidants. Oxidative Medicine and Cellular Longevity, **2021**, *2021*.
113. Benelli, G. Mode of action of nanoparticles against insects. *Environ. Sci. Pollut. Res.* **25**, 12329–12341. https://doi.org/10.1007/s11356-018-1850-4 (2018).
114. Murugan, K. et al. Eco-friendly drugs from the marine environment: Spongeweed-synthesized silver nanoparticles are highly effective on Plasmodium falciparum and its vector Anopheles stephensi, with little non-target effects on predatory copepods. *Environ. Sci. Pollut. Res.* **23**, 16671–16685. https://doi.org/10.1007/s11356-016-6832-9 (2016).
115. Hashem, A. H. et al. Unveiling Antimicrobial and Insecticidal Activities of Biosynthesized Selenium Nanoparticles Using Prickly Pear Peel Waste. *J. Functional Biomater.* **13**, 112 (2022).
116. Soni, N.; Prakash, S.J.T.S.W.J. Green nanoparticles for mosquito control. **2014**, *2014*, 496362.
117. Veerakumar, K. & Govindarajan, M. Adulticidal properties of synthesized silver nanoparticles using leaf extracts of Feronia elephantum (Rutaceae) against filariasis, malaria, and dengue vector mosquitoes. *Parasitol. Res.* **113**, 4085–4096. https://doi.org/10.1007/s00436-014-4077-4 (2014).
118. Benelli, G. Plant-mediated synthesis of nanoparticles: A newer and safer tool against mosquito-borne diseases?. *Asian Pac. J. Trop. Biomed.* **6**, 353–354. https://doi.org/10.1016/j.apjtb.2015.10.015 (2016).

119. Suresh, U. et al. Tackling the growing threat of dengue: Phyllanthus niruri-mediated synthesis of silver nanoparticles and their mosquitocidal properties against the dengue vector Aedes aegypti (Diptera: Culicidae). *Parasitol. Res.* **114**, 1551–1562. https://doi.org/10.1007/s00436-015-4339-9 (2015).
120. Roni, M. et al. Characterization and biotoxicity of Hypnea musciformis-synthesized silver nanoparticles as potential eco-friendly control tool against Aedes aegypti and Plutella xylostella. *Ecotoxicol. Environ. Saf.* **121**, 31–38. https://doi.org/10.1016/j.ecoenv.2015.07.005 (2015).
121. Madhiyazhagan, P. et al. Sargassum muticum-synthesized silver nanoparticles: an effective control tool against mosquito vectors and bacterial pathogens. *Parasitol. Res.* **114**, 4305–4317. https://doi.org/10.1007/s00436-015-4671-0 (2015).
122. Barik, T. K., Kamaraju, R. & Gowswami, A. Silica nanoparticle: a potential new insecticide for mosquito vector control. *Parasitol. Res.* **111**, 1075–1083. https://doi.org/10.1007/s00436-012-2934-6 (2012).

Author contributions

Alsayed E. Mekky.: Conceptualization, Methodology, Resources, Software; Writing-original draft; Ebrahim Saied.: Conceptualization, Formal analysis, Investigation, methodology, Writing-original draft, Writing-review and editing.; Mahmoud M. Al-Habibi: Conceptualization, Data curing, Formal analysis; Zeinab A. Shouaib.: Conceptualization, Investigation, Visualization, Validation; Ahmed I. Hasaballah.: Data curing, Formal analysis, Validation, Visualization,. Mohammed E. Rashed: Investigation, methodology, Resources; Ashjan F. Khalel: Formal analysis, Investigation, methodology; Amal Naif Alshammari: Resources, Software; Fady Sayed Youssef: Conceptualization, Software, Validation, Visualization, analysis, Writing-review and editing; Ahmed M. Al-Shahat: Data curing, Software, Validation; Mohammad Y. Alfaifi: Conceptualization, Methodology, Resources, Software; Writing-original draft; Serag Eldin Elbehairy: Conceptualization, Methodology, Resources, Software; Writing-original draft; Mohammed Aufy: Conceptualization, Methodology, Resources, Software; Writing-original draft, writing final draf; Tharwat A. Selim: Visualization, Writing-original draft, Writing -review and editing.

Funding

The authors extend their appreciation to the Deanship of Research and Graduate Studies at King Khalid University for funding this work through Large Research Project under grant number RGP.2/361/45.

Declarations

Competing interests

The authors declare no competing interests.

Ethical approval

The study received ethical approval from the Faculty of Science Research Ethics Board (FSR 15,162,118).

Additional information

Supplementary Information The online version contains supplementary material available at https://doi.org/10.1038/s41598-025-11838-6.

Correspondence and requests for materials should be addressed to M.A. or T.A.S.